Accepted Manuscript

Journal of the Geological Society

The Provenance of Middle Jurassic to Cretaceous sediments in the Irish and Celtic Sea Basins: Tectonic and Environmental controls on sediment sourcing

Odhrán McCarthy, Brenton Fairey, Patrick Meere, David Chew, Aidan Kerrison, David Wray, Mandy Hofmann, Andreas Gärtner, Benita-Lisette Sonntag, Ulf Linnemann & Klaudia F. Kuiper

DOI: https://doi.org/10.1144/jgs2020-247

To access the most recent version of this article, please click the DOI URL in the line above. When citing this article please include the above DOI.

Received 11 December 2020
Revised 11 March 2021
Accepted 17 March 2021

Supplementary material at https://doi.org/10.6084/m9.figshare.c.5343657

Full Title: The Provenance of Middle Jurassic to Cretaceous sediments in the Irish and Celtic Sea Basins: Tectonic and Environmental controls on sediment sourcing

Abbreviated title: Celtic and Irish Seas Mesozoic basin provenance

Odhrán McCarthy[1*], Brenton Fairey[2], Patrick Meere[1], David Chew [3], Aidan Kerrison[4], David Wray[5], Mandy Hofmann[6], Andreas Gärtner[6], Benita-Lisette Sonntag[6], Ulf Linnemann[6], Klaudia F. Kuiper[7]

[1]School of Biological, Environmental and Earth Sciences and iCRAG, University College Cork

[2]Chemostrat, Welshpool, United Kingdom

[3]Department of Geology and iCRAG, Trinity College Dublin, Dublin, Ireland

[4]School of Earth and Atmospheric Sciences, Queensland University of Technology, Brisbane, QLD, Australia

[5] School of Science, University of Greenwich, Kent, UK, ME4TB

[6]Senckenberg Naturhistorische Sammlungen Dresden, Museum für Mineralogie und Geologie, Königsbrücker Landstraße 159, D-01109 Dresden, Germany

[7]Department of Earth Sciences, Vrije Universiteit Amsterdam, De Boelelaan 1085, NL-1081 HV Amsterdam, The Netherlands

ORCiDs of authors preceded by their initials:

O.M. 0000-0002-6940-1035

P.M. 0000-0001-7686-2641

B.F. 0000-0002-8506-2192

D.C. 0000-0002-6940-1035

D.W. 0000-0002-0799-2730

A.G. 0000-0002-1670-7305

K.K. 0000-0001-6345-5019

Correspondence: odhranm04@hotmail.com

Abstract: The Jurassic and Cretaceous sedimentary infill of the Irish and Celtic Sea basins is intimately associated with the breakup of the supercontinent Pangea, and the opening of the Atlantic margin. Previous basin studies have constrained tectonism, basin uplift and sediment composition, but sediment provenance and routing have not received detailed consideration. Current hypotheses for basin infill suggest localised sediment sourcing throughout the Jurassic and Cretaceous, despite a dynamic tectonic and paleoenvironmental history spanning more than 100 million years. We present detrital zircon, white mica and apatite geochronology alongside heavy mineral data from five basins. Findings reveal that basin infill derived predominantly from distal sources with lesser periods of local sourcing. We deduce that tectonically induced marine transgression and regression events had a first-order control on distal *versus* proximal sedimentary sourcing. Additionally, tectonism which uplifted the Fastnet Basin region during the Middle–Late Jurassic recycled basin sediments into the connected Celtic and Irish Sea Basins. Detrital geochronology and heavy mineral evidence support three distinct provenance switches throughout the Jurassic and Cretaceous in these basins. Overall an integrated multi-proxy provenance approach provides novel insights to tectonic and environmental controls on basin infill as demonstrated in the Irish and Celtic Sea Basins.

Keywords: Provenance, North Celtic Sea Basin, Saint George's Channel Basin, Cimmerian Tectonism, U-Pb dating, Ar-Ar dating, Heavy Mineral Analysis

Provenance investigations provide useful insights into important environmental and tectonic events as well as the origin and routing of sediments. This is especially true for the Mesozoic sedimentary basins of the Irish and Celtic Seas, which formed after the rifting and breakup of the palaeocontinent Pangea, and during the protracted opening of the Atlantic margin (Naylor and Shannon 1982; Allen *et al.* 2002). Previous research has primarily focused on the basin tectonics and structure, hydrocarbon potential and paleoenvironmental history, furthering our understanding of the evolution of this offshore segment of the Atlantic Margin (Shannon 1991; Shannon *et al.* 2001; Naylor and Shannon 2011). Evidence of more than two kilometres of basin exhumation during the Jurassic and Cretaceous indicates that tectonism played an integral role in the sourcing, routing and preservation of the basin infill (Cogné *et al.* 2014; Cogné *et al.* 2016; Rodríguez-Salgado *et al.* 2019). However, there is a distinct gap in our understanding of the interplay of environmental and tectonic controls on the provenance of the Irish Mesozoic basin infill. Despite more than 40 years of economic exploration in the Jurassic and Cretaceous successions, there have been no dedicated provenance studies in the North Celtic Sea Basin (NCSB) (Fig. 1), Saint George's Channel Basin (SGCB), South Celtic Sea Basin (SCSB), Fastnet Basin and Goban Spur Basin (O'Reilly *et al.* 1991; Shannon 1996). Sediment is thought to have been locally derived from the Upper Devonian Munster Basin and the adjacent, Early to Middle Paleozoic, Leinster Massif (Fig. 1) throughout the Jurassic and Cretaceous (Robinson *et al.* 1981; Ainsworth *et al.* 1985; Millson 1987; Caston 1995; Naylor and Shannon 2011). However, while this simple model is consistent with biostratigraphic data, sedimentary petrography, paleocurrent data and seismic investigations, these observations provide limited insight into the detailed sedimentary provenance. Considering the active tectonism and fluctuating environmental signals observed in the region during the Mesozoic (Naylor and Shannon 2011), it seems unlikely that only two sediment sources were active throughout the Jurassic and Cretaceous Periods. Given that the major tectonic and environmental events that shaped these basins are well-constrained, the basins make for an ideal testing ground for investigating the effects of such events on sediment provenance.

The study area includes five sedimentary basins on the continental shelf off the coast of southeast Ireland in the Irish and Celtic Seas (Fig. 1). Mesozoic and Cenozoic stratigraphy in the study area has been truncated by multiple exhumation events driven by either; i) epeirogenic mechanisms related to the proto-Iceland plume (Brodie and White 1994; Jones *et al.* 2002; Cogné *et al.* 2016) or, ii) far-field tectonic influences from the Mesozoic Cimmerian (Early Alpine) orogeny (Rawson and Riley 1982), and the Cenozoic Alpine orogeny (Ziegler *et al.* 1995). These first order tectonic controls on basin development drove localised marine transgression-regression cycles throughout the Mesozoic Period. Recently, a revised stratigraphic nomenclature was proposed for Irish offshore stratigraphy (ISPSG 2019) and is incorporated into Fig. 2, which summarises the stratigraphy, tectonism and sea level change in the SGCB, NCSB and Fastnet Basin. Of the 105 wells drilled across these basins, 35 samples were taken from Jurassic and Cretaceous sandstone units across 19 wells. Investigating the provenance of these basins is challenging as numerous potential paleocontinental sources yield similar detrital zircon populations (e.g. Peri-Gondwanan sources such as Avalonia, Megumia, Iberia and Armorica) requiring alternative analytical techniques like apatite and mica geochronology or feldspar analysis for diagnostic source fingerprinting. Such

techniques have been successfully applied in the Slyne (Franklin *et al.* 2020), Munster (Fairey 2017), Dingle (Fairey *et al.* 2018) and Clare basins (Nauton-Fourteu *et al.* 2020) in the Irish offshore and mainland.

This study aims to test the hypothesis that the Leinster Massif and Munster Basin were the primary sediment sources throughout the Middle Jurassic to Late Cretaceous in the North Celtic Sea Basin (NCSB), Saint George's Channel Basin (SGCB), Fastnet Basin and Goban Spur Basin (Fig. 1). Additionally, we aim to better characterise the influence of tectonic and environmental controls on sediment provenance in the study area. A multi-proxy approach of single grain geochronology (U-Pb zircon and apatite, and $^{40}Ar/^{39}Ar$ mica dating), apatite trace element analysis and bulk sediment characterisation of heavy mineral abundance (HMA) was undertaken. To contextualise changes in sediment provenance during basin development, sandstones within larger stratigraphical units which mark potentially significant changes in tectonic and environmental conditions were sampled (see Fig. 2 and Table 7 of supplementary materials for further detail). More broadly, findings of this study could have implications for other basins along the Atlantic Margin.

GEOLOGICAL BACKGROUND

Overview

The NCSB is linked to the SGCB to the north, and Fastnet Basin and South Celtic Sea Basin to the south (Fig. 1). It records the thickest (9 km maximum thickness) stratigraphic succession of Mesozoic stratigraphy (Rodriguez-Salgado 2019) of these basins and is well profiled with 2D and 3D seismic surveys (Sibuet *et al.* 1990; O'Reilly *et al.* 1991; Rodríguez-Salgado *et al.* 2019), 88 drilled wells as well as gravity and magnetic surveys (Sibuet *et al.* 1990). The Fastnet Basin (16 wells in total) preserves a limited succession of Middle – Upper Jurassic stratigraphy due to Cimmerian uplift (Fig. 2), but was an important igneous centre throughout the Mesozoic Era (Caston *et al.* 1981; Ainsworth *et al.* 1985; Murphy and Ainsworth 1991; Ewins and Shannon 1995). The SGCB contains a complete section of Triassic and Jurassic stratigraphy but has limited Cretaceous successions due to Cenozoic exhumation and erosion. The Goban Spur Basin is the least studied of these basins with only one well, and limited 2D and 3D seismic survey data (Yang *et al.* 2020). Generally, offshore well records tend to focus on Cretaceous intervals across the Irish and Celtic Sea, and of the 114 wells drilled in the Celtic Sea, only 26 penetrate basement rock. Due to limited well penetration, numerous unconformities, and poor quality 2D seismic data, the Jurassic and Triassic stratigraphy of these units is only partially understood in the study area.

Pre-Mesozoic to Early Jurassic Tectonic Framework

Basin development offshore of the south and east of Ireland (the Celtic and Irish Sea basins) initiated towards the end of the Carboniferous and into the early Permian and was associated with the breakup of the supercontinent of Pangea (Chadwick and Evans 1995). By the Early Triassic, renewed rifting of Pangea followed a northeast-southwest Caledonian structural fabric in the region (Shannon 1991) (Fig. 1). The Early Triassic basins are interpreted to have been disconnected, long and narrow and of varying size and were located 15 – 20° north of the equator with an arid climate (Warrington and Ivimey-Cook 1992). By the Late Triassic to Early Jurassic, rift chains extended along Pangea from the

Tethys Ocean to the central Atlantic. These rift chains were associated with further development of early Permian – Triassic rift basins, and deepening transgressive marine conditions resulting in the deposition of the Mercia Mudstone Group throughout the study area (Ruffell and Shelton 1999).

Open marine conditions developed during the latest Triassic to Early Jurassic resulting in the deposition of the Lias Group (Fig. 2), with regional transgressive marine sedimentation during the Rhaetian slowing and shallowing into carbonate dominated marine environments by the Hettangian. The study area had drifted north to a latitude of c. 30° by the Early – Middle Jurassic (Bassoulet 1993). Marine conditions persisted until a thermal subsidence induced regression event in the Late Sinemurian led to the deposition of localised deltaic and shallow marine sandstones along the margins of the SGCB, northern NCSB and Fastnet Basin (Naylor and Shannon 2011). Terrestrial clastic sediment is thought to have been sourced from the Old Red Sandstone of the Munster Basin or the Fastnet Spur during the Sinemurian, while the eastern half of the NCSB is thought to have sourced sediment from the Leinster Massif (Petrie *et al.* 1989). There then followed a localised transgression back into mixed, shallow marine carbonate and sandstone deposition by the Pliensbachian (Kessler and Sachs 1995). The SGCB is thought to have received input from the Leinster Massif at this time as the progradation of deltaic and shallow marine clastic sediments feeding from the Leinster Massif switched from south to east (Petrie *et al.* 1989). The Toarcian brought a widespread, thermal subsidence-related transgression, resulting in mudstone and shale deposition throughout the Celtic Sea basins (Murphy and Ainsworth 1991).

Middle to Late Jurassic sedimentation and Cimmerian tectonism

Middle Jurassic sedimentation was strongly affected by the onset of Cimmerian tectonism which exerted a strong control on exhumation and relative sea level changes (C1 uplift, Fig. 2) in the Celtic and Irish Sea basins (Ziegler 1990). In this study, Cimmerian tectonism refers to the pulsed, far-field effects of the Cimmerian orogeny of central Asia and Mediterranean-Alpine Europe, which was associated with the closure of Palaeotethys and opening of Neotethys (Stampfli and Kozur 2006). It is linked to stages of rift-related, Middle Jurassic to Late Cretaceous tectonism, initiating in the Aalenian as outlined by Naylor and Shannon (2011) and Rodríguez-Salgado *et al.* (2019) in the study area. Continued regression during the Aalenian developed thick nearshore deltaic sequences in the east, and argillaceous and calcareous sand beds in the west of the SGCB. Sea level started to rise into the Late Bajocian, likely because of thermal subsidence, and argillaceous deposits became more frequent (Eagle Group, Fig. 2). More than 700 m of Middle Jurassic successions (Lias – Hook Groups) are preserved in the NCSB. The Fastnet Basin preserves 233 m (well 56/26-1) of the Middle Jurassic Eagle Group which was exhumed and eroded later in in the Middle Jurassic by Cimmerian tectonism (Fig. 2). During the Bajocian, six sills and possible volcanic plugs intruded along northeast-trending fault zones in the Fastnet Basin (Caston *et al.* 1981; Rodríguez-Salgado *et al.* 2019). During the Bathonian, a localised marine regression resulted in shallow marine conditions in the northeast NCSB and SGCB, where bioclastic sands were deposited as part of the Eagle Group. Carbonate shelves developed in the NCSB and SGCB and shallow marine conditions developed in the Cardigan Bay Basin (Fig. 1) (Caston 1995).

During the Bathonian, another phase of Cimmerian tectonism uplifted and eroded Middle to Upper Jurassic successions in the Fastnet Basin and the western margin of the NCSB (Fig. 2.).

Though speculative, a hot spot may have caused doming of the Goban Spur Basin, Fastnet Basin and western NCSB which drove uplift and erosion (Shannon 1996), while the SGCB and northern NCSB remained as marine environments with deposition of calcareous mud, silt and thin intervals of sand (325 m Well 50/3-2 & 700 m Well 103/2-1). Sedimentation has been interpreted as syn-rift, continental to shallow marine in origin, possibly sourced from the re-activated basin margins including the Munster Basin, Leinster, Cornubian and Welsh massifs (Fig. 1). Rising sea levels and progressive rifting produced marine conditions in the NCSB and SGCB. A further regressive event developed during the Late Bathonian, resulting in a freshwater to a brackish environment throughout the Irish Sea. The Callovian – Oxfordian is marked by deposition of cross bedded, current rippled and braided fluvial sediments of the Hook Group (1157 m Well 50/3-2) in most areas of the NCSB which rest unconformably (Fig. 2) on carbonaceous Bathonian strata as a result of Cimmerian tectonism. The Fastnet Basin records 433 m (Well 63/8-1) of the Hook Group. Sediment sourcing during this period is thought to have been derived from the exhumed and eroded basin margins in the NCSB (Caston 1995). The SGCB had a marginal marine-lacustrine environment at this time comprising calcareous muds interbedded with sparse sandstones and occasionally fluvial braided sequences. Evidence of fault-bounded sedimentation in a warm and wet palaeo-climate is provided by non-marine, *Classopollis* pollen and red oxidised kaolinite-smectite dominated clays in Middle – Upper Jurassic sediment on the southeast Irish mainland (Higgs and Beese 1986), which contrasts with the thick, clastic sequences developed in the adjacent offshore. During the Oxfordian – Tithonian, the facies distribution changed from fluvial drained sediments to increasingly lacustrine/marginal-marine in the NCSB. Throughout this period, the SGCB remined a marginal – marine environment depositing, carbonate-rich sands, silts and calcareous mudstone units (Naylor and Shannon 2011).

Cretaceous sedimentation

Crustal extension along Atlantic fault systems occurred at the Jurassic – Cretaceous boundary as part of a late phase of Cimmerian tectonism (Rawson and Riley 1982). Consequently, in the vicinity of southern Ireland, continental shelves and upland areas were exhumed (C2 uplift Fig. 2) along with the adjacent offshore basins (Rodríguez-Salgado *et al.* 2019). This coincided with a fall in sea level globally from the Tithonian – Valanginian (Haq 2014). Marginal basin areas were eroded, and continental, fluvial and deltaic sediments were deposited, as part of the Purbeck Group, lying unconformably upon Upper Jurassic successions in the Irish and Celtic Sea regions (Fig. 2). The Purbeck units contain non-marine, white – pink, fine-coarse grained sandstone with greenish grey calcareous claystones and marls (Caston 1995). These units have an average thickness of 230 m across the basins and a maximum thickness of 560 m (well 57/2-2). Brackish – freshwater Berriasian sediments were followed by Valanginian – Hauterivian alluvial shales, while fluvial sandstones likely derived from a western source, like the Leinster Massif and Munster Basin, are also identified in the Fastnet Basin and NCSB (Robinson *et al.* 1981; Ainsworth *et al.* 1985). The study area was in a mid-latitude region at the time (Allen 1981; Culver and Rawson 2006), closer to its current latitude, and observed a change from arid to humid climate conditions during the Valanginian (Ruffell and Rawson 1994). A global transgression (Haq 2014) in the Hauterivian – Albian is recorded by deposition across much of the Irish and Celtic Seas, of the marginal-marine to marine Wealden Group (Rowell 1995) and later the Selbourne Group and

coincides with a period post-rift thermal subsidence (Fig. 2). Marine conditions continued into the Cenomanian, resulting in regional deposition of the Chalk Group (1200 m thick well 93/2-1, and 191 m well 50/2-1) (Payton 1977; Haq 2014). Later, during the Cenozoic, the basin margins were exhumed and eroded as part of the initial phase of prolonged uplift and subsidence associated with the opening of the Atlantic (Anell *et al.* 2009). This uplift event removed Upper Jurassic and Cretaceous material from the SGCB producing major unconformities overlain by Cenozoic strata (Fig. 2). Throughout the Cretaceous, periods of igneous activity in the Porcupine Basin, Western Approaches, Goban Spur Basin and Fastnet Basin (Fig. 2) were common and typically coincided with rifting phases in the Atlantic and opening of the Bay of Biscay, while the NCSB, SCSB and SGCB regions were volcanically quiescent throughout the Mesozoic (Croker and Shannon 1987; Tate and Dobson 1988; García-Mondéjar 1996; Rodríguez-Salgado *et al.* 2019). The common occurrence of unconformities, and the evident removal of basin margins is crucial in this investigation as potential proximal sediment sources, available during the Jurassic and Cretaceous, are no longer preserved in the geological record.

POTENTIAL SEDIMENT SOURCES

Potential sediment sources are considered in terms of tectonostratigraphic domains (Hibbard *et al.* 2007) as their unique geological histories help to determine the ultimate source of the Mesozoic infill. The exact boundaries, and tectonic history of each domain are continually debated (Waldron *et al.* 2019b). Two broad palaeocontinental assemblages can be found in Britain and Ireland. These are Laurentian (and Peri-Laurentian) domains north of the Iapetus Suture, and Peri-Gondwanan domains to the south (Fig. 1) (Hibbard *et al.* 2007; Pollock *et al.* 2012). Peri-Gondwanan domains are separated into Ganderia, the Monian Composite Terrane, Avalonia and Megumia (Waldron *et al.* 2019b). More recent tectonomagmatic events are also included in the characterisation of source regions as they further help in fingerprinting sources (e.g. Permian igneous activity within Avalonia).

Laurentia

Laurentian crustal provinces in the North Atlantic region comprise amalgamated Archean-Paleoproterozoic cratonic blocks such as the North Atlantic Craton in Greenland and Eastern Canada (Buchan *et al.* 2000). In Ireland and Britain Laurentian sources include the Lewisian Complex (2.9 – 1.7 Ga) (Rainbird *et al.* 2001; McAteer *et al.* 2014), the Annagh Gneiss Complex (1.8 – 1.0 Ga)(Daly and Flowerdew 2005) of northwest Ireland and the Rhinns Complex (1.8 – 1.7 Ga) of northern Ireland and Scotland (Daly 1996; Chew and Strachan 2014). Broadly, Laurentian domains have been affected by Archean, the Trans-Hudson/Nagssugtoqidian (2.0 – 1.8 Ga)(Hoffman 1990; Henrique-Pinto *et al.* 2017), Labradorian (1.7 – 1.6 Ma), Pinwarian (1.5 – 1.4 Ga) (Gower 1996; McAteer *et al.* 2014), and Grenville (1.3 – 0.9 Ga) orogenic events. Not all of these orogenic phases affected the Laurentian basement units in Britain and Ireland, but many of these orogenic episodes are typically captured by detrital zircon ages in Laurentian cover sequences. In Scotland and Ireland, these cover sequences include the Neoproterozoic Moine Supergroup and Neoproterozoic to Early Paleozoic Dalradian Supergroup, which both exhibit a broad range of detrital zircon populations from 3.1 – 0.9 Ga characteristic of a Laurentian provenance (See Chew and Strachan (2014)). The Laurentian Caledonides of Scotland and Ireland were

intruded by a series of granitic bodies from 470 - 400 Ma, with the major peak in granitic magmatism at 430 – 400 Ma (Miles and Woodcock 2018; Murphy *et al.* 2019).

Peri – Laurentia

Peri-Laurentia, refers to the domain along the southeastern Laurentian margin which is associated with subduction and closure of the Iapetus Ocean (McConnell *et al.* 2016). The Southern Uplands – Longford-Down Terrane is bounded by the Southern Uplands Fault to the north, and the Iapetus Suture to the south in Ireland and northern Britain (Fig. 1). Detrital zircon spectra from the Southern Uplands terrane are comprised of 2.0 – 0.9 Ga Laurentian zircon with a particularly prominent 1.5 – 1.0 Ga population, with Ordovician 490 – 470 Ma zircon becoming more prominent in the southern tracts (Waldron *et al.* 2014). Permian to Carboniferous extensional volcanism in the Midland Valley of southern Scotland is dated from 342 – 329 Ma by the $^{40}Ar/^{39}Ar$ method, with a shorter-lived second phase at c. 298 Ma (Monaghan and Pringle 2004; Kirstein *et al.* 2006). The Southern Upland Terrane is thus comprised of sediment primarily derived from Laurentia and includes Paleozoic magmatic detritus.

Peri-Gondwanan domains

The Peri-Gondwanan domain includes all terranes that were proximal to the northern margin of western Gondwana during the Early Neoproterozoic until the breakup of Gondwana in the early Paleozoic (Van der Voo 1988; Nance *et al.* 2008). These domains include Ganderia, Megumia, the Monian Composite Terrane, Avalonia and Cadomia, and are a source of abundant 525 – 690 Ma zircon (Pothier *et al.* 2015).

Ganderia and the Monian Composite Terrane

To the immediate south of the Iapetus Suture in Ireland and Britain lies Ganderia, sometimes referred to as Avalonia (Tyrrell *et al.* 2007; Fullea *et al.* 2014; Todd 2015) and more rarely Cadomia in the literature (Soper and Hutton 1984; Max *et al.* 1990). The Leinster Massif is an important potential source area. It is comprised of Neoproterozoic basement (the Rosslare Complex) intruded by the Saint Helens Gabbro (618 Ma), the Saltees Granite (437 Ma), the Carrigmore Diorite (415 Ma) and three intrusive phases of the Leinster Batholith (417, 409 and 404 Ma) (Brück *et al.* 1974; O'Connor and Brück 1978; Long *et al.* 1983; Max *et al.* 1990; Fritschle *et al.* 2018). The Leinster Massif forms part of the Leinster-Lakesman Terrane, an eastward extension of the Ganderian terrane of Newfoundland. It has long been considered a likely source of recycled material into the Irish and Celtic Sea regions (Winn Jr 1994; Hartley 1995; Taber *et al.* 1995; Naylor and Shannon 2011). Zircon populations from these Ganderian domains are typically dominated by 700 – 500 Ma and c. 400 Ma populations, often with subordinate 2.2 – 1.0 Ga Amazonian populations (Strachan *et al.* 2007). The Monian Composite Terrane incorporates the Isle of Anglesey and the southern margin of the Leinster Massif (Fig. 1) (Waldron *et al.* 2014; Pothier *et al.* 2015; Waldron *et al.* 2019a). Like Ganderia, this terrane represents a significant source of metamorphic and igneous detritus with U-Pb detrital zircon populations similar to those of Ganderia.

Megumia

The term “Megumia” was suggested by Waldron *et al.* (2011) for the Meguma Terrane in Nova Scotia and the Harlech Dome in Wales because of their similar biostratigraphy and

geochronological signatures and the existence of this domain is further supported by the work of White *et al.* (2012) and Nance *et al.* (2015). Avalonia and Megumia are challenging sources to distinguish using detrital zircon geochronology alone (Collins and Buchan 2004; Strachan *et al.* 2007; Pothier *et al.* 2015). The Welsh Massif was likely an important sediment source region for the Celtic Sea basins and incorporated the Megumian domain to the north and the Avalonian domain to the south (Fig. 1).

Avalonia

Avalonia in southern England is identified as Caledonian 'East Avalonia' (as opposed to Appalachian 'West Avalonia') and typically is a source for abundant 540 – 650 Ma detrital zircon grains (Waldron *et al.* 2019b). For a more detailed description of the distinction between East versus West Avalonia see van Staal *et al.* (1996) and Pothier *et al.* (2015). Topographic highs of Avalonian basement during the Mesozoic include the Cornubian Massif and the London-Brabant High (Fig. 1). The Cornubian Massif also contains post-Variscan extrusive and intrusive igneous rocks (Smith *et al.* 2019).

Cadomia

Cadomia includes terranes of the southern Variscan Belt, the Armorican Massif in north-western France and the Iberian Massif in Spain. For a detailed description of these Cadomian terranes see Nance *et al.* (2008) and Henderson *et al.* (2016). The Iberian and Armorican Massif contains Cambrian marine sediments overlying Neoproterozoic volcano-sedimentary successions. The Variscan Orogeny resulted in regional metamorphism of these crustal blocks and the emplacement of associated igneous intrusions (Guerrot and Peucat 1990; Dallmeyer *et al.* 2013). These domains would be expected to yield abundant Variscan, Paleozoic and Neoproterozoic zircon and mica, like other Peri-Gondwanan domains in NW Europe (Fernández-Suárez *et al.* 2000; Gutiérrez-Alonso *et al.* 2005).

Post-Caledonian cover sequences

Important cover sequences which are likely sources of recycled Peri-Gondwanan and Laurentian material to the Celtic and Irish Sea basins include the Dingle Basin (Fairey *et al.* 2018), the Upper Devonian Munster Basin, the Carboniferous Clare Basin (Nauton-Fourteu *et al.* 2020) and other coeval clastic sequences in central Ireland . The Munster Basin comprises an Upper Devonian to Lower Carboniferous volcano-sedimentary succession affected by Variscan orogenesis (Meere and Mulchrone 2006). Fairey (2017) demonstrated that the Upper Devonian Old Red Sandstone of the Munster Basin typically contains two distinct U-Pb zircon populations including; i) Silurian (c. 430 Ma) and Grenville (1.0 Ga) populations which appear to have a Laurentian affinity (e.g. the Gyleen and Kiltorcan formations) and ii) Silurian and Peri-Gondwanan (c. 700 Ma) populations with subordinate 0.9 – 2.2 Ga populations (e.g. the Harryloch Formation). The former of these two populations appears to be the most common in the Munster Basin, making it challenging to differentiate from Laurentian sources. In addition, Visean volcanism was sporadically developed in central Ireland (c. 337 Ma) and was broadly coeval with volcanism in the Midland Valley of Scotland (Somerville *et al.* 1992). Apatite fission track data from the Galtee Mountains, Lugnaquilla and Mount Leinster record three phases of onshore exhumation during the Triassic – Early Jurassic (200-170 Ma), Jurassic-Cretaceous boundary (c. 145 Ma) and Early Cretaceous (c. 110 Ma) and comprised a total of 1.5 – 3 km of exhumation over 150 Ma (Cogné *et al.* 2016).

METHODS

Rationale

A multi-proxy approach of single grain geochronology (U-Pb zircon and apatite, and $^{40}Ar/^{39}Ar$ mica dating), apatite trace element analysis and bulk sediment characterisation of HMA was undertaken in this study to minimise analytical bias and to capture diverse metamorphic, igneous and sedimentary sources (Hietpas *et al.* 2011; Chew *et al.* 2020). Due to limited sample size, the conventional approach of splitting samples for heavy mineral and geochronology analysis was not possible. Heavy mineral concentrates were mounted in resin directly after separation and mapped via Qualitative Evaluation of Minerals by Scanning Electron Microscopy (QEMSCAN) analysis for mineral identification and subsequent U-Pb geochronology (Pascoe *et al.* 2007; Zhang *et al.* 2015). Six core and 27 drill cutting samples were taken from the core stores of the Irish Petroleum Affairs Division (PAD) in Dublin and the British Geological Survey Core Shed in Keyworth, UK (see supplementary data table 7).

Sample Preparation

Zircon, Apatite and Heavy Mineral Analysis

Processing of samples was conducted at University College Cork (UCC), Ireland. Samples from core and drill cuttings were cleaned by thoroughly washing samples through a < 250 µm sieve and then cleaned with an ultrasonic bath to remove remaining clay material. Samples were disaggregated using a jaw crusher and sieved into 63 – 125 µm and 125 – 250 µm grain size fractions where the 63 – 125 was chosen for heavy mineral analysis (Morton 1984; Mange and Maurer 1992; Morton and Hallsworth 1994). Density separation was conducted with lithium polytungstate (density ca 2.85 $g.cm^{-3}$) by centrifuge and recovered by partial freezing with liquid nitrogen (Garzanti 2017). Where the recovered heavy fraction was large enough, the cone and quarter method was used to reduce samples for mounting. Samples were then mounted on double-sided sticky tape, cast in epoxy resin and grains were ground and polished to half thickness. Samples are labelled by basin where NC indicates the North Celtic Sea Basin, SG - Saint George's Channel Basin, SC - South Celtic Sea Basin, GS - Goban Spur Basin and FB - the Fastnet Basin. Fifteen Zircon and four mica samples NC1, NC6 - NC8, NC17 – NC20, NC26&NC27, SC1, GS1 and FB1 – FB6 were processed and analysed as in Fairey et al. (2018) (see Table 2). Zircon U-Pb geochronology is commonly utilized in provenance studies as zircon has a high closure temperature of >900 °C, is resistant to weathering and chemical alteration effects, and can be analysed with rapid sample throughput (Gehrels *et al.* 2006; Chew *et al.* 2017; Vermeesch *et al.* 2017). However, zircon has a natural fertility bias wherein it is under-represented in mafic and some metamorphic sources (Hietpas *et al.* 2011). To capture zircon-poor sources, a combination of detrital white mica and apatite geochronology was also undertaken. The combination of apatite trace element analysis and U-Pb geochronology (closure temperature window of c. 375 – 550 °C) is effective in identifying the age and composition of both igneous and metamorphic sources (O'Sullivan *et al.* 2020).

White Mica

White mica samples were prepared in the geochronology laboratory, Vrije Universiteit Amsterdam, Amsterdam, Netherlands. Grains were disaggregated by jaw crusher and disc mill. To preserve coarse grains, sieving took place between incrementally decreasing crush sizes. Grains of 200 – 500 µm were retained after each sieving step. Mica-rich samples were further processed using a shaking table to concentrate platy minerals. Samples with a poor mica yield were further separated by density separation using diluted diiodomethane with a density of 2.78 g/cm^{-3}in an overflow centrifuge. A Franz magnetic separator was used to remove magnetic and paramagnetic impurities. Finally, grains for $^{40}Ar/^{39}Ar$ geochronology were handpicked under an optical microscope to avoid inclusions or impurities. White mica has a closure temperature of 445 – 400 °C (Harrison *et al.* 2009), is a good indicator of metapelite, felsic igneous and hydrothermal sources (Mange and Wright 2007), and is often considered a first order source indicator as it is liable to mechanical disaggregation in aeolian settings, although is more durable in a subaqueous setting (Anderson *et al.* 2017).

Heavy Mineral Analysis

Twenty-one samples from the Jurassic and Cretaceous successions of the northern NCSB and SGCB were processed for heavy mineral analysis. After mounting, samples were ground and polished to half thickness and processed for QEMSCAN analysis at 10 µm resolution by Rocktype Ltd in their Oxford laboratory. The FEI-trademarked QEMSCAN® technique is an automated mineralogy method which combines Energy Dispersive Spectroscopy (EDS) with software that enables automated pixel by pixel spectral acquisition and post-analysis mineral classification. Drill cuttings can sometimes be contaminated with drilling additives or caved materials, and it is important to note that datasets derived from these sources can sometimes be contaminated and should be interpreted with caution (see Table 7 for full sample details). Core samples (which do not experience this effect) are identified throughout the text and in figures for this reason. Upon reviewing mud logs, the minerals barite and fluorite which are commonly encountered in drilling mud were excluded from the HMA results with the remaining phases normalised to 100 %. Raman spectroscopy was used to differentiate between kyanite, sillimanite and andalusite and between REE phosphate minerals at University College Cork (UCC). A Renishaw inVia™ confocal Raman microscope with a 50 mW DPSS (diode-pumped, solid-state) 532 nm laser, at 1 second residence time, 10 % laser strength and a 50x objective was used for these spot analyses. Raman spectra were identified using the RUFF database (Lafuente *et al.* 2015) and in-house libraries. Mineral phases considered as provenance indicator minerals include zircon, tourmaline, TiO_2 phases, apatite, sphalerite, garnet, titanite, monazite, clinopyroxene, kyanite, staurolite and chrome-spinel. Other phases include abundant pyrite, chalcopyrite, biotite, muscovite and siderite. Once classified, light phases were excluded and heavy mineral groups were normalised to 100% of the total HMA (Zhang *et al.* 2015). The reported total volume percentage of mineral abundance from the QEMSCAN analysis can introduce biases as naturally larger minerals (e.g. tourmaline) have a higher modal volume than if point counting was undertaken. QEMSCAN analysis also does not differentiate between authigenic and detrital or mineral polymorphs which can also introduce bias; the influence of these biases was considered when interpreting the heavy mineral results. Heavy mineral GZi (garnet vs zircon) and MZi (monazite vs zircon) indices were calculated following Morton and Hallsworth (1994).

Geochronology

Zircon and Apatite U-Pb dating

A maximum of up to 175 zircon grains in four samples were randomly selected and their positions on grain mounts located in UCC using a Renishaw inVia™ confocal Raman microscope. Zircon and apatite isotopic analysis was conducted using an Agilent 7900 Quadrupole ICPMS coupled to a Photon Machines Analyte Excite 193 nm ArF Excimer laser ablation system with a Helex 2-volume ablation cell at the Department of Geology, Trinity College Dublin. The spot size was 24 µm and 30 µm spots for zircon and apatite analysis, respectively. The primary reference materials were Plešovice zircon (Sláma *et al.* 2008) and Madagascar apatite (Wiedenbeck *et al.* 1995; Thomson *et al.* 2012) respectively. The weighted mean ^{206}Pb-^{238}U ages for secondary zircon standards are: in-house zircon standard WRS 1348 (Pointon *et al.* 2012) = 529.4 ± 2.6 Ma (n = 50), 91500 zircon (Wiedenbeck *et al.* 1995) = 1055.1 ± 4.6 Ma (n=42) and GZ7 (Nasdala *et al.* 2018) = 528.6 ± 2.0 Ma (n=50). The ^{207}Pb-corrected apatite secondary standard ages are: McClure Mountain (Schoene and Bowring 2006) = 526.3 ± 4.7 Ma (n=38) and Durango (McDowell *et al.* 2005) = 30.4 ± 1.0 Ma (n=45). When compared with the published reference age values, all results are within 2σ uncertainty of their published ages. Reduction of raw isotope data was conducted in Igor Pro software with the Iolite 2.5 package extension. The primary standards Madagascar apatite and Plešovice zircon were used to correct for mass bias, downhole U-Pb fractionation and intra-session instrument drift using the data reduction schemes' VisualAge' for zircon and 'VisualAge_UcomPbine' for apatite (Paton *et al.* 2011; Petrus and Kamber 2012; Chew *et al.* 2014; Chew *et al.* 2019a). Apatite is a challenging mineral to accurately date as it can incorporate high levels of common lead (Pb_c) during crystallisation which can result in high Pb_c to radiogenic lead (Pb*) ratios. An iterative Pb_C correction was employed for all detrital apatite unknowns after Chew *et al.* (2014). As apatite often yields large U-Pb age uncertainties, particularly in grains with high Pb_c / Pb* ratios, the results were filtered using an age dependent uncertainty threshold (Chew *et al.* 2020), with a 2σ uncertainly filter of 50% employed for grains younger than 100 Ma, 15% for 100-1000 Ma and 5% for 1.0 – 3.6 Ga. To maximise precision, zircon single grain concordia ages were calculated using the Isoplot v4.15 Excel add for all zircon samples in this study (Ludwig 2012). Concordant ages for zircon are displayed for a probability of concordance > 0.001 (Zimmermann *et al.* 2018). Kernel density estimate (KDE) curves were plotted using IsoplotR (Vermeesch 2018). A 25 Ma bandwidth was chosen for zircon and apatite to limit over smoothing and facilitate cross-sample comparison.

Zircon sample NC22a was analysed in the Department for Science, University of Greenwich. U-Pb LA-ICP-MS analysis was conducted using a Thermo Scientific iCAP Q Quadrupole ICP-MS coupled to an Elemental Scientific NWR213 laser ablation unit fitted with a TwoVol2 ablation chamber. Calibration was achieved using the zircon 91500 reference material which was measured after every 10 unknown grains throughout the measurement run. Accuracy was independently verified by regular measurement of the Plešovice zircon standard, which was treated as an unknown. The weighted mean value of Plešovice single grain ages was calculated at 339.0 ± 4.0 Ma (n=30) and is within published uncertainties (Sláma *et al.* 2008). A 25 µm spot size was used. Optimum grain sampling during the unattended run was maintained via the use of 'Imagelock' within the laser ablation software platform. The resultant measurements were processed with Iolite v3.7 using its U_Pb_Geochron4 data

reduction scheme. Zircon samples NC1, NC6 – NC8, NC17 – NC21, GS1 and FB1 – FB5 were processed following Fairey *et al.* (2018), from unpublished PhD data.

Detrital White Mica

Four white mica samples were irradiated together with Fish Canyon sanidine (FCs) for 18 hours at the Oregon State University TRIGA reactor in the cadmium-shielded CLICIT facility. $^{40}Ar/^{39}Ar$ analyses were performed at the geochronology laboratory of the VU University on a Helix MC noble gas mass spectrometer. Single mica grains were fused with a Synrad CO_2 laser beam and released gas was exposed to NP10 and St172 getters and analysed on the Helix MC. The five argon isotopes were measured simultaneously with ^{40}Ar on the H2-Faraday position with a 10^{13} Ω resistor amplifier, ^{39}Ar on the H1-Faraday with a 10^{13} Ω resistor amplifier, ^{38}Ar on the AX-CDD (CDD – Compact Discrete Dynode), ^{37}Ar on the L1-CDD and ^{36}Ar on the L2-CDD. Gain calibration for the CDDs are done by peak jumping a CO_2 reference beam on all detectors in dynamic mode. All intensities are corrected relative to the L2 detector. Air pipettes are run every ten hours and are used for mass discrimination corrections. The atmospheric air value of 298.56 from Lee *et al.* (2006) is used. Detailed analytical procedures for the Helix MC are described in Monster (2016). The calibration model of Kuiper *et al.* (2008) with an FCs age of 28.201 ± 0.046 Ma and the decay constants of Min *et al.* (2000) are used in age calculations. The correction factors for neutron interference reactions are (2.64± 0.02) $x10^{-4}$ for $(^{36}Ar/^{37}Ar)^{Ca}$, (6.73 ± 0.04) $x10^{-4}$ for $(^{39}Ar/^{37}Ar)^{Ca}$, (1.21 ±0.003) $x10^{-2}$ for $(^{38}Ar/^{39}Ar)^{K}$ and (8.6 ± 0.7) $x10^{-4}$ for $(^{40}Ar/^{39}Ar)^{K}$. All uncertainties are quoted at the 2σ level and include all analytical errors. A 25 Ma bandwidth was chosen for mica to limit over smoothing and facilitate cross-sample comparison with zircon and apatite.

Apatite Trace Elements

During U-Pb isotope analysis of apatite, trace element concentrations were simultaneously obtained. The primary standard employed used was NIST 612 standard glass, and a crushed aliquot of Durango apatite, whose trace element abundances are characterised by solution ICP-MS (Chew *et al.* 2016), was used as a secondary standard. The trace element data were reduced using the Iolite "Trace Elements" data reduction scheme. The apatite trace element chemistry was interrogated using the approach of O'Sullivan *et al.* (2020), which employs Support Vector Machine (SVM) discrimination to a literature database of apatite-bedrock compositions. This method allows the user to utilise the light rare earth element (LREE, sum of La-Nd) and Sr/Y trace element data collected during U-Pb analysis to differentiate between alkali-rich igneous rocks (ALK), mafic I-type granitoids and mafic igneous rocks (IM), low- and medium-grade metamorphic and metasomatic rocks (LM), partial-melts, leucosomes and high-grade metamorphic rocks (HM), S-type and high aluminium saturation index, 'felsic' I-types granitoids (S) and ultramafic rocks including carbonatites, lherzolites and pyroxenites (UM) (O'Sullivan et al., 2020). The apatite trace element analyses are then plotted on a bivariate (sum LREE vs Sr/Y plot), with each analysis coloured according to its ^{207}Pb-corrected age (Fig. 7). Grains which fail the uncertainty threshold are coloured grey.

RESULTS

Heavy mineral datasets from 21 samples are summarised in Fig. 3. Kernel density estimate (KDE) diagrams of age data from 1144 zircon (15 samples), 214 mica (4 samples) and 176 apatite grains (3 samples including trace element data) from the NCSB, SGCB, Fastnet and

Goban Spur Basins are presented. The age data are grouped into six tectonomagmatic populations to facilitate sample comparison (Table 1). These include grain populations - P1; Atlantic rift-related volcanism, P2; Variscan and Acadian, P3; Caledonian, Scandian and Grampian, P4; Peri-Gondwanan, P5; Grenvillian and Pinwarian and P6; Labradorian and Lewisian (see potential sediment sources section for references). It is important to note that the zircon, apatite and mica yield in some samples is limited, and the age data from these small populations should be interpreted with caution. Samples NC7, NC8, NC11, NC17, NC19 and SG5 are from core samples while the remainder are drill cuttings.

Heavy Mineral Analysis

QEMSCAN analysis of 21 heavy mineral separates characterised between 137 – 7993 heavy mineral grains per sample. These results are summarised as a percentage of total volume in Fig. 3 (Zhang *et al.* 2015). Three out of 21 samples contained less than 200 grains (137; 177; 188) and may not fully represent the heavy mineral population (Morton 1982). Mineral ratios were calculated after Morton and Hallsworth (1994) where mineral counts were substituted for total volume %. In addition, multivariate principal component analysis (PCA) using the R package "Provenance" was chosen to identify mineral correlations (Vermeesch *et al.* 2016) (Fig. 4). TiO_2 polymorphs like anatase/brookite as well as sphalerite are common authigenic phases (Mange and Maurer 1992) and have not been differentiated from authigenic and detrital phases. Therefore, TiO_2 phases may represent authigenic (anatase/brookite) or detrital (rutile) grains.

Middle Jurassic – Upper Jurassic Samples

Middle Jurassic sediments of the SGCB comprise abundant TiO_2 phases, apatite, tourmaline, garnet and zircon with some clinopyroxene, sphalerite, monazite and titanite in places (Fig. 3). Upper Jurassic samples of the SGCB contain abundant apatite, tourmaline and garnet with limited TiO_2 phases and sphalerite. Upper Jurassic samples of the NCSB have abundant zircon, tourmaline, TiO_2 phases and apatite with some garnet and traces of sphalerite, titanite and staurolite indicative of a metamorphic, igneous or hydrothermal source. Upper Jurassic samples from the SGCB generally contain less zircon and more tourmaline, garnet and sphalerite than those of the NCSB.

Cretaceous Samples

The Lower Cretaceous samples NC23 – NC25 (Wells 50/03-01 and 50/03-02) are composed of 18% to >42% apatite along with TiO_2 phases, tourmaline and garnet. Limited zircon and chrome spinel make up the remainder of the samples, like the Upper Jurassic samples of the SGCB (Fig. 3 and Fig. 4). Principal component analysis of the heavy mineral data shows that the Lower Cretaceous samples positively correlate with PC1 because of the increase in staurolite and kyanite. The Upper Cretaceous sample NC22 (Well 50/07-01) also contains significant apatite and TiO_2 phases but with a marked increase in staurolite and kyanite. Sample SG16 (Well 106/28-1) also contains abundant TiO_2 phases and apatite, with more clinopyroxene than any other sample from the NCSB or SGCB (Fig. 4). This further supports the presence of a proximal igneous source.

Principal component analysis of the HMA data is summarised in Fig. 4A. PC1 correlates positively with clinopyroxene and apatite and to a lesser extent with sphalerite and garnet and negatively correlates with zircon, TiO_2 phases, chrome spinel and monazite. As

sphalerite is positively correlated with garnet and tourmaline, it is likely from a metamorphic or igneous source, but may also be related to authigenic growth. Kyanite, apatite, zircon and clinopyroxene positively correlate with PC2 and there is a strong negative correlation with garnet, sphalerite and tourmaline. The PCA and MZi *vs* GZi ratio plots successfully distinguish the garnet-rich and zircon-poor Late Jurassic sediments of the SGCB from all other samples (Fig. 4b).

Zircon U-Pb Geochronology

Middle Jurassic

The Middle Jurassic (Callovian) sample GS1 (Well 62/07-1) from the Goban Spur Basin has a dominant c. 1.7 Ga (Labradorian – Lewisian) population (Fig. 5). Caledonian – Grampian zircon, and some Archean and Grenville grains comprise the rest of the sample population. The Bathonian sample SG5 (core from Well 107/16-1) from the SGCB contains a dominant Grenville population centred around 1.0 Ga with some Pinwarian and Archean detritus. In both samples, the absence of significant late Neoproterozoic zircon is noteworthy and indicates an absence of Peri-Gondwanan input.

Upper Jurassic

The Upper Jurassic samples NC6 (Well 49/15-1), NC7 (core from Well 49/9-3), NC8 (core from Well 49/10-1), NC9a (Well 50/03-1) and NC10 (Well 50/03-02) from the NCSB share similar diverse zircon U-Pb age populations from 0.4 to 2.7 Ga, with abundant sub-peaks (Fig. 5). Unlike the Middle Jurassic samples above, zircon of Peri-Gondwanan affinity is abundant in all samples. Core sample NC7 contains a young 176 Ma zircon population (n = 3).

Cretaceous

The Variscan – Acadian (P2) and Caledonian – Scandian – Grampian populations (P3) dominate in the Lower Cretaceous (Valanginian – Barremian) zircon samples NC18 (Well 48/18-1), NC19 (Core sample, Well 48/24-4), NC20 (Well 48/28-1), NC26 (Well 56/22-1) and FB4 (Well 56/26-2). These samples lack significant Grenville – Pinwarian (P5) and Labradorian – Lewisian (P6) U-Pb zircon populations, which marks an important provenance switch compared to the Jurassic samples (Fig. 6). The Albian sample NC17 (Well 49/9-2) comprises mostly Proterozoic, Peri-Gondwanan (P4) and Caledonian (P3) grains with a single 128 Ma zircon, the youngest zircon found in this study, and broadly mirrors the zircon age population seen in the Campanian sample NC22 (Well 50/07-01). Samples NC22 and NC17 lack a 2.0 Ga population and have subordinate Peri-Gondwanan and dominant Paleozoic populations.

Apatite U-Pb Geochronology and trace elements

Middle Jurassic

Apatite from the Bathonian core sample SG5 comprises a multi-source trace element signature (Fig. 7). The broadly syn-depositional (230 – 160 Ma) population has a mixed mafic/I-type granite affinity, while the 280 – 320 Ma Variscan grains have a mafic/I-type granite affinity along with apatite grains derived from low-grade metamorphic rocks. Older (late Grenville, c. 900 Ma) apatites have a mixed metamorphic and igneous affinity. The

majority of the ultramafic and low-grade metamorphic apatite resulted in ages with large uncertainties which fail the U-Pb age uncertainty filter and are hence underrepresented in the U-Pb geochronology KDE plots (Fig. 7C). The absence of Mesoproterozoic and older apatite in this sample is noteworthy compared to the zircon age spectra from the same sample while the younger 300 – 160 Ma sources are clearly underrepresented in the zircon populations of SG5 (Fig. 5). The youngest apatite age population in sample SG5a suggests an active igneous source of ultramafic-mafic affinity in or near the NCSB and SGCB during the Middle – Late Jurassic (See Table 4); this is only poorly recorded in the zircon dataset (e.g. a sub-population at 176 Ma in core sample NC7, Fig. 5).

Cretaceous

Cenomanian apatite sample SG16 (Well 106/28-1) contains Scandian – Caledonian and syn-depositional Cretaceous populations with distinct c. 95 Ma and c. 420 Ma peaks. Apatite trace element plots for this sample show a mafic/I-type igneous signature for all grains with two distinct populations within this field on the SVM plot (Fig. 7A). In sample NC22 (Well 50/07-01), the apatite is derived from a single Cretaceous (c. 95 Ma) population with a mafic to ultramafic igneous affinity. The abundant Cretaceous apatite (and a single zircon dated at 128 Ma in sample NC17) demonstrate a syn-depositional igneous source unrecognised in the NCSB and SGCB to date.

White Mica Ar-Ar Geochronology

Jurassic core sample NC7 (Well 49/9-03), along with Cretaceous samples NC19 (core from Well 48/24-4) and NC17 (Well 49/9-02) yield white mica of late Caledonian or Acadian affinity (main peak at 435 Ma), an age peak which is also detected in zircon populations of the NCSB (Fig. 8). The Valanginian sample NC27 (Well 56/15-01) located toward the southern margin of the NCSB contains a slightly younger Caledonian – Acadian population (395 Ma) with an additional Peri-Gondwanan sub-population and a single white mica dated at 1423 Ma.

DISCUSSION

Middle Jurassic Provenance

During the Middle Jurassic, the initial phases of far-field Cimmerian tectonism uplifted the entire southern margin of the study area (Rodríguez-Salgado *et al.* 2019). Heavy mineral assemblages from the SGCB indicate a metamorphic, igneous or hydrothermal source for these sediments (Fig. 3). The Callovian sample GS1 from the Goban Spur Basin, and the Bathonian core sample SG5 from the SGCB, were deposited prior to or during this uplift event when the Irish and Celtic Sea regions were connected (Fig. 9). U-Pb Zircon populations in these samples differ, with the Goban Spur sample GS1 exhibiting a dominant 1.7 Ga Proterozoic KDE peak while the SGCB has an asymmetric series of Proterozoic KDE peaks culminating in a 1.0 Ga Grenville population (Fig. 5).

This Grenville population in the SGCB (core sample SG5) is likely sourced predominantly from the north. A c. 1.9 – 1.0 Ga zircon population is prominent in the Longford Down – Southern Uplands terrane and the Silurian sequences of the Lake District (Waldron *et al.* 2014) (see

Fig. 5). The apatite U-Pb data (sample SG5) also support dominant north-derived input into the SGCB, as 275 Ma mafic/I-type granitoids are indicative of the Midland Valley Terrane of the Scottish Massif (Monaghan and Pringle 2004). The c. 900 Ma (late Grenville) apatite is likely derived from a northern source – either the Southern Uplands – Longford Down terrane (for which no apatite U-Pb data are available), or from portions of the Laurentian basement which record post-Grenville cooling with no significant Caledonian (*sensu lato*) tectonothermal overprinting (Fig. 7C). The c. 170 Ma ultramafic – mafic apatite is likely sourced from Middle Jurassic volcanism in the Fastnet Basin (Caston *et al.* 1981), suggesting a dominant northern and subordinate southern input to the SGCB (Fig. 9). If these magmatic sources were eroded and the resulting sediment transported by marine currents or littoral drift into the SGCB, this would indicate inter-basin connectivity, but a pyroclastic origin is also possible (Fig. 7C). Material from the Goban Spur Basin (GS1) has a more prominent 1.7 Ga population. This dominant Laurentian signature in GS1 is likely from a Laurentian source to the north, of which the most proximal sources would include the Dalradian Supergroup (Chew *et al.* 2010), Rhinns Complex, or granitic orthogneisses of the Porcupine High (Chew *et al.* 2019b). Importantly, Late Neoproterozoic populations in GS1 and SG5 are either minor or absent. This indicates that there was minimal sourcing from Cadomia to the south or from recycling of post-Caledonian cover sequences of onshore Ireland such as the Leinster Massif and Clare Basin (Morton *et al.* 2016; Nauton-Fourteu *et al.* 2020). Potential sourcing from the Upper Devonian Munster Basin is more difficult to establish. The Upper Old Red Sandstone of the Munster Basin contains little Neoproterozoic detrital zircon and abundant Silurian and Grenville detrital zircon (Fairey 2017), similar to sample SG5. Thus it is not possible to definitively rule out this potential source as a significant contributor of Laurentian detrital zircon in this sample. However when the detrital zircon data are combined with the U-Pb and trace element data and the heavy mineral abundance results, a more distal northern source region is thought more likely.

Late Jurassic Provenance

By the Late Jurassic, Cimmerian exhumation had established a land barrier which separated the Celtic and Irish Sea Basins from the Goban Spur Basin (Fig. 10). Uplift in the SGCB region resulted in shallow marine conditions while the NCSB persisted as an open marine environment. Sediment is thought to have been derived from the basin margins producing sand-prone marine carbonates, and continental fluvial deposits with limited basin connectivity in the Irish and Celtic Sea Regions (Caston 1995; Naylor and Shannon 2011). The HMA principal component analysis, and MZI and GZI ratios show that Middle Jurassic samples in the SGCB (SG5, SG12, SG13 and SG15) and Upper Jurassic samples in the NCSB (NC9 – NC11 and NC13 – NC16) are rich in zircon and TiO_2 phases (albeit some may be authigenic), while Upper Jurassic samples in the SGCB (SG7 – SG10) are zircon-poor and tourmaline- and garnet-rich and are highly distinctive on the PCA and MZI *vs* GZI plots (Fig. 4). These results signal a provenance switch from the Middle to Upper Jurassic in the SGCB, and that the NCSB and SGCB were likely not connected during the Late Jurassic. The negative correlation with PC1, and positive correlation with PC2 of the Middle Jurassic SGCB and Upper Jurassic NCSB HMA samples in Fig. 4A, indicates a similar provenance of mixed metamorphic, igneous and recycled sedimentary successions.

The Upper Jurassic NCSB U-Pb detrital zircon spectra (NC6 – NC10) contain diverse Laurentian 2.9 – 0.9 Ga populations, but also, significantly, a prominent c. 700 Ma Peri-

Gondwanan population. Comparatively, Bathonian sample SG5 (Fig. 5) contains dominant Grenville and subordinate Peri-Gondwanan and Labradorian U-Pb zircon populations supporting the Middle – Late Jurassic provenance switch observed in SGCB HMA samples. This implies that the Leinster Massif and Welsh Massif, which contain dominant Peri-Gondwanan populations (Waldron *et al.* 2014; Pothier *et al.* 2015) and the uplifted Fastnet Basin and onshore Munster Basin, which containing mixed Laurentian and Peri-Gondwanan populations, were potential sources into the NCSB. Assuming the Oxfordian (154.78 Ma – 161.53 Ma, timescale of Hesselbo (2020)) biostratigraphic age assigned to sample core NC7 is accurate, then the small but conspicuous 176 Ma zircon population present in this sample (weighted average age of three grains = 176.6 ± 1.9 Ma) supports recycling from the Fastnet Basin, as no other intrusive or volcanic body of this age is found in the surrounding area (Caston *et al.* 1981). These findings partially support local sediment sourcing as proposed by Caston (1995), with an additional, previously unrecognised, component of recycled detritus from the uplifted Fastnet Basin region.

Early Cretaceous Provenance

A late phase of Cimmerian tectonism induced a regression during the Early Cretaceous causing fluvial sedimentation of the Purbeck and Wealden Groups in the Irish and Celtic Sea Basins (Rodríguez-Salgado *et al.* 2019) (Fig. 11). Exhumation of the Leinster Massif and Munster Basin regions was also ongoing throughout this period (Cogné *et al.* 2016). Heavy mineral samples from the northern margin of the NCSB (NC23 – NC25) contain abundant apatite and TiO_2 phases, some tourmaline, staurolite, sphalerite, zircon and limited kyanite, monazite and titanite. This broadly reflects input from igneous and metamorphic sources, supporting sediment derivation from the Monian Composite Terrane, and Welsh and Leinster Massifs (Fig. 4). U-Pb zircon and Ar-Ar mica results from the Early Cretaceous (Valangian – Barremian) sequences (NC18 – NC20, NC26, SC1 and FB4) contain dominant Neoproterozoic – Palaeozoic and subordinate 2.9 – 0.9 Ga (Laurentian) detrital zircon populations (Fig. 6 & 8), indicating sourcing from the Munster Basin (Fairey 2017), Welsh Massif (Pothier *et al.* 2015) and/or Leinster Massifs (Waldron *et al.* 2014). This therefore supports earlier models such as Robinson *et al.* (1981) and Ainsworth *et al.* (1985) that proposed sediment sourcing from western sources like the Munster Basin and Leinster massif. The decrease in Laurentian-derived populations in the Early Cretaceous is attributed to a marine regression disconnecting Laurentian sources with the Celtic Sea, and tectonic quiescence limiting inter-basin recycling.

During the Albian, sedimentation was significantly influenced by transgressive conditions initiated by post-rift related thermal subsidence (Taber *et al.* 1995) (Fig. 12). Isopach, sediment facies and petrographic analysis on the Greensand and Wealden/Selbourne groups by Winn Jr (1994), Taber *et al.* (1995) and Hartley (1995) suggest that sediment was sourced locally from reworked Wealden Group to the south, or the Leinster and Welsh massifs and the Munster Basin. Detrital zircon U-Pb spectra from the Albian core sample NC17 (Well 49/9-2) comprises an asymmetric 1.1 Ga Grenville population, and a significantly reduced Neoproterozoic (peri-Gondwanan) population compared to the underlying Valanginian – Barremian sequences. This population is likely sourced from the Gyleen Formation of the Munster Basin (Fairey 2017) proximal to the sample site of NC17 (Well 49/9-2) which has a Laurentian provenance, or more distally from the Southern Uplands – Longford Down terrane (cf Waldron *et al.* (2014); Fig. 5). These data do not support reworking from the

Wealden Group, Leinster or Welsh Massifs, as these units are all characterised by prominent Peri-Gondwanan zircon peaks (e.g. see Wealdon Group samples NC18 – NC20 in Fig. 6).

Late Cretaceous Provenance

By the Turonian, initial deposition of the Chalk Group had begun as transgressive conditions progressed across northern Europe (Fig. 12) (Hancock 1989). U-Pb apatite and trace element analysis combined with HMA data from samples SG16 and NC22 indicates an ultramafic-mafic source region with continuous igneous activity from 130 – 85 Ma such as is found in the Porcupine, Goban Spur and Fastnet Basins mixed with older Caledonian sources like the Leinster and Welsh Massifs. The presence of kyanite, garnet and staurolite indicates an additional metamorphic source. Additionally, the abundance of apatite with an igneous trace element chemistry in NC22 and SG16 support a significant magmatic source. Given that the detrital zircon spectrum from NC22 favours a Laurentian source, the metamorphic source terrane is more likely a terrane with a Laurentian affinity such as the Dalradian Supergroup in northwest Ireland possibly transported by long-distance marine mechanisms into the Celtic Sea, like the ultra-long distance littoral transport observed along the west coast of Namibia (Garzanti *et al.* 2014). The Munster Basin likely contributed some Laurentian detritus to these late Cretaceous sequences also (Fig. 6A). The dominance of Laurentian zircon in sample NC22 and NC17 (core sample) likely indicates sourcing from the Dalradian metasediments of western Ireland and possibly the Munster Basin. The syn-depositional Cretaceous apatite population in samples NC22 and SG16, are probably tuffs associated with magmatic centres in the Fastnet, Porcupine or Goban Spur basins. Fastnet Basin or another rift-related magmatic sources in the region.

CONCLUSIONS

Transgression – regression cycles and Cimmerian tectonism exhibited strong control on distal *versus* proximal sediment sourcing in the Irish and Celtic Sea Basins during the Middle Jurassic to Late Cretaceous. Recycling of sediments from the Munster Basin into the offshore domain remains a significant provenance challenge and requires a multi-proxy provenance approach. These controls resulted in three distinct provenance switches demonstrating that sediment did not principally derive from local sources. These findings suggest the following:

1. Laurentian-derived sediment was the dominant source in the connected Goban Spur Basin, Fastnet Basin, NCSB and SGCB during the Middle Jurassic.
2. Possible derivation from a Middle Jurassic volcanic source in the Fastnet basin is identified in the SGCB implying basin connectivity or ash fall sedimentation into the surrounding basins.
3. Late Jurassic Cimmerian tectonism reworked strata from the Fastnet Basin and marginal basin regions into the Celtic sea and SGCB inhibiting sediment exchange between the NCSB and SGCB.
4. Fluvial sedimentation during the Early Cretaceous drained from the Irish and Welsh Massifs into the NCSB, SCSB, SGCB, and Fastnet Basins.
5. During a transgression in the Late Cretaceous, Laurentian-derived sediment likely transported from the Dalradian Supergroup of western Ireland by marine mechanisms into the NCSB and SGCB, along with pyroclastic deposits from syn-rift ultramafic-mafic magmatism.

Acknowledgments

F. Drakou is thanked for assistance in analysing detrital apatite and zircon samples for U-Pb geochronology. G. Summers and A. du Vahin are thanked for help in processing and generating Raman maps of zircon grains. J. Omma is thanked for analysis of heavy mineral samples. G. O'Sullivan and M. Naughton are thanked for their advice in data processing and analysis.

Funding

O.McC, P.M, and D.C acknowledge the financial support of Science Foundation Ireland, Grant/Award Number: 13/RC/2092; European Regional Development Fund; PIPCO RSG. This publication uses data and survey results acquired during a project undertaken on behalf of the Irish Shelf Petroleum Studies Group (ISPSG) of the Irish Petroleum Infrastructure Programme (PIP) Group 4 (project code IS 12/05 UCC). The ISPSG comprises Atlantic Petroleum (Ireland) Ltd, Cairn Energy Plc, Chrysaor E&P Ireland Ltd, Chevron North Sea Limited, ENI IrelandBV, Europa Oil&Gas, ExxonMobil E&P Ireland (Offshore) Ltd, Husky Energy, Kosmos Energy LLC, Maersk Oil North Sea UK Ltd, Petroleum Affairs Division of the Department of Communications, Energy and Natural Resources, Providence Resources Plc, Repsol Exploración SA, San Leon Energy Plc, Serica Energy Plc, Shell E&P Ireland Ltd, Sosina Exploration Ltd, Tullow Oil Plc and Woodside Energy (Ireland) Pty Ltd.

Appendices

All supplementary material can be found in Excel spreadsheet Tables 2 – 7:

- Table 2-Heavy Minerals
- Table 3- Zircon U-Pb Geochronology
- Table 4-Apatite U-Pb Geochronology
- Table 5-Apatite Trace elements
- Table 6-White Mica
- Table 7-Sample list of all sample locations, depths and types

References

Ainsworth, N.R., Horton, N.F. and Penney, R.A. 1985. Lower Cretaceous micropalaeontology of the Fastnet Basin, offshore south-west Ireland. *Marine and Petroleum Geology*, **2**, 341-349, https://doi.org/https://doi.org/10.1016/0264-8172(85)90029-7.

Allen, P. 1981. Pursuit of Wealden models. *Journal of the Geological Society, London*, **138**, 375-405, https://doi.org/https://doi.org/10.1144/gsjgs.138.4.0375.

Allen, P.A., Bennett, S.D., Cunningham, M.J.M., Carter, A., Gallagher, K., Lazzaretti, E., Galewsky, J., Densmore, A.L., Phillips, W.E.A., Naylor, D. and Hach, C.S. 2002. The post-Variscan thermal and denudational history of

Ireland. *Geological Society, London, Special Publications*, **196**, 371-399, https://doi.org/10.1144/gsl.sp.2002.196.01.20.

Anderson, C.J., Struble, A. and Whitmore, J.H. 2017. Abrasion resistance of muscovite in aeolian and subaqueous transport experiments. *Aeolian Research*, **24**, 33-37, https://doi.org/https://doi.org/10.1016/j.aeolia.2016.11.003.

Anell, I., Thybo, H. and Artemieva, I. 2009. Cenozoic uplift and subsidence in the North Atlantic region: Geological evidence revisited. *Tectonophysics*, **474**, 78-105, https://doi.org/https://doi.org/10.1016/j.tecto.2009.04.006.

Bassoulet, J.-P., Elmi, S., Poisson, A., Cecca, F., Bellion, Y., Guiraud, R., Baudin, F.,. 1993. Middle Toarcian (184-182 Ma). *In*: Dercourt, J., Ricou, L.E., Vrielynck, B. (ed.) *Atlas Tethys Paleoenvironmental Maps*. Gauthier-Villars, Paris, 63-84.

Brodie, J. and White, N. 1994. Sedimentary basin inversion caused by igneous underplating: Northwest European continental shelf. *Geology*, **22**, 147-150, https://doi.org/https://doi.org/10.1130/0091-7613(1994)022<0147:SBICBI>2.3.CO;2.

Brück, P., Potter, T.L. and Downie, C. 1974. The Lower Palaeozoic stratigraphy of the northern part of the Leinster Massif. *Proceedings of the Royal Irish Academy. Section B: Biological, Geological, and Chemical Science.* JSTOR, 75-84.

Buchan, K., Mertanen, S., Park, R., Pesonen, L., Elming, S.-Å., Abrahamsen, N. and Bylund, G. 2000. Comparing the drift of Laurentia and Baltica in the Proterozoic: the importance of key palaeomagnetic poles. *Tectonophysics*, **319**, 167-198, https://doi.org/https://doi.org/10.1016/S0040-1951(00)00032-9.

Caston, V. 1995. The Helvick oil accumulation, Block 49/9, North Celtic Sea Basin. *Geological Society, London, Special Publications*, **93**, 209-225, https://doi.org/10.1144/gsl.sp.1995.093.01.15.

Caston, V., Dearnley, R., Harrison, R., Rundle, C. and Styles, M. 1981. Olivine-dolerite intrusionsin the Fastnet Basin. *Journal of the Geological Society, London*, **138**, 31-46, https://doi.org/https://doi.org/10.1144/gsjgs.138.1.0031.

Chadwick, R. and Evans, D. 1995. The timing and direction of Permo-Triassic extension in southern Britain. *Geological Society, London, Special Publications*, **91**, 161-192, https://doi.org/https://doi.org/10.1144/GSL.SP.1995.091.01.09.

Chew, D., Drost, K. and Petrus, J.A. 2019a. Ultrafast,> 50 Hz LA-ICP-MS Spot Analysis Applied to U–Pb Dating of Zircon and other U-Bearing Minerals. *Geostandards and Geoanalytical Research*, **43**, 39-60, https://doi.org/https://doi.org/10.1111/ggr.12257.

Chew, D., O'Sullivan, G., Caracciolo, L., Mark, C. and Tyrrell, S. 2020. Sourcing the sand: Accessory mineral fertility, analytical and other biases in detrital U-Pb provenance analysis. *Earth-Science Reviews*, 103093, https://doi.org/https://doi.org/10.1016/j.earscirev.2020.103093.

Chew, D., Tyrrell, S., Daly, J.S., Cogné, N., Sun, K. and Badenszki, E. 2019b. The Basement geology of the Porcupine High - A Key Transatlantic link between the Caledonides and Apalachians. *GSA Annual Meeting in Phoenix, Arizona, USA-2019.* GSA.

Chew, D.M. and Strachan, R.A. 2014. The Laurentian Caledonides of Scotland and Ireland. *Geological Society, London, Special Publications*, **390**, 45-91, https://doi.org/https://doi.org/10.1144/SP390.16.

Chew, D.M., Petrus, J.A. and Kamber, B.S. 2014. U–Pb LA–ICPMS dating using accessory mineral standards with variable common Pb. *Chemical Geology*, **363**, 185-199, https://doi.org/https://doi.org/10.1016/j.chemgeo.2013.11.006.

Chew, D.M., Petrus, J.A., Kenny, G.G. and McEvoy, N. 2017. Rapid high-resolution U–Pb LA-Q-ICPMS age mapping of zircon. *Journal of Analytical Atomic Spectrometry*, **32**, 262-276, https://doi.org/https://doi.org/10.1039/C6JA00404K.

Chew, D.M., Daly, J.S., Magna, T., Page, L.M., Kirkland, C.L., Whitehouse, M.J. and Lam, R. 2010. Timing of ophiolite obduction in the Grampian orogen. *Bulletin*, **122**, 1787-1799, https://doi.org/https://doi.org/10.1130/B30139.1.

Chew, D.M., Babechuk, M.G., Cogné, N., Mark, C., O'Sullivan, G.J., Henrichs, I.A., Doepke, D. and McKenna, C.A. 2016. (LA, Q)-ICPMS trace-element analyses of Durango and McClure Mountain apatite and implications for

making natural LA-ICPMS mineral standards. *Chemical Geology*, **435**, 35-48, https://doi.org/https://doi.org/10.1016/j.chemgeo.2016.03.028.

Cogné, N., Chew, D. and Stuart, F.M. 2014. The thermal history of the western Irish onshore. *Journal of the Geological Society, London*, **171**, 779-792, https://doi.org/https://doi.org/10.1144/jgs2014-026.

Cogné, N., Doepke, D., Chew, D., Stuart, F.M. and Mark, C. 2016. Measuring plume-related exhumation of the British Isles in Early Cenozoic times. *Earth and Planetary Science Letters*, **456**, 1-15, https://doi.org/https://doi.org/10.1016/j.epsl.2016.09.053.

Collins, A. and Buchan, C. 2004. Provenance and age constraints of the South Stack Group, Anglesey, UK: U–Pb SIMS detrital zircon data. *Journal of the Geological Society, London*, **161**, 743-746, https://doi.org/https://doi.org/10.1144/0016-764904-036.

Croker, P. and Shannon, P. 1987. The evolution and hydrocarbon prospectivity of the Porcupine Basin, offshore Ireland. *Conference on petroleum geology of North West Europe. 3*, 633-642.

Culver, S.J. and Rawson, P.F. 2006. *Biotic response to global change: the last 145 million years*. Cambridge University Press.

Dallmeyer, R.D., Franke, W. and Weber, K. 2013. *Pre-Permian geology of central and eastern Europe*. Springer Science & Business Media.

Daly, J.S. 1996. Pre-Caledonian history of the Annagh Gneiss Complex North-Western Ireland, and correlation with Laurentia-Baltica. *Irish Journal of Earth Sciences*, 5-18.

Daly, J.S. and Flowerdew, M.J. 2005. Grampian and late Grenville events recorded by mineral geochronology near a basement–cover contact in north Mayo, Ireland. *Journal of the Geological Society, London*, **162**, 163-174, https://doi.org/https://doi.org/10.1144/0016-764903-150.

EMODnet, B.C. 2018. EMODnet Digital Bathymetry (DTM 2018).

Ewins, N.P. and Shannon, P.M. 1995. Sedimentology and diagenesis of the Jurassic and Cretaceous of the North Celtic Sea and Fastnet Basins. *Geological*

Society, London, Special Publications, **93**, 139-169, https://doi.org/https://doi.org/10.1144/GSL.SP.1995.093.01.12.

Fairey, B.J. 2017. *Sediment routing and recycling through multiple basins from Palaeozoic to Mesozoic times: a provenance study of the Devonian Old Red Sandstone of southern Ireland and neighbouring offshore Mesozoic basins.* PhD thesis, University College Cork.

Fairey, B.J., Kerrison, A., Meere, P.A., Mulchrone, K.F., Hofmann, M., Gärtner, A., Sonntag, B.-L., Linnemann, U., Kuiper, K.F. and Ennis, M. 2018. The provenance of the Devonian Old Red Sandstone of the Dingle Peninsula, SW Ireland; the earliest record of Laurentian and peri-Gondwanan sediment mixing in Ireland. *Journal of the Geological Society, London*, jgs2017-2099, https://doi.org/https://doi.org/10.1144/jgs2017-099 |.

Fernández-Suárez, J., Gutiérrez-Alonso, G., Jenner, G. and Tubrett, M. 2000. New ideas on the Proterozoic-Early Palaeozoic evolution of NW Iberia: insights from U–Pb detrital zircon ages. *Precambrian Research*, **102**, 185-206, https://doi.org/https://doi.org/10.1016/S0301-9268(00)00065-6.

Franklin, J., Tyrrell, S., O'Sullivan, G., Nauton-Fourteu, M. and Raine, R. 2020. Provenance of Triassic sandstones in the basins of Northern Ireland—Implications for NW European Triassic palaeodrainage. *Geological Journal*, https://doi.org/https://doi.org/10.1002/gj.3697.

Fritschle, T., Daly, J.S., Whitehouse, M.J., McConnell, B. and Buhre, S. 2018. Multiple intrusive phases in the Leinster Batholith, Ireland: geochronology, isotope geochemistry and constraints on the deformation history. *Journal of the Geological Society, London*, **175**, 229-246, https://doi.org/https://doi.org/10.1144/jgs2017-034.

Fullea, J., Muller, M., Jones, A. and Afonso, J. 2014. The lithosphere–asthenosphere system beneath Ireland from integrated geophysical–petrological modeling II: 3D thermal and compositional structure. *Lithos*, **189**, 49-64, https://doi.org/https://doi.org/10.1016/j.lithos.2013.09.014.

García-Mondéjar, J. 1996. Plate reconstruction of the Bay of Biscay. *Geology*, **24**, 635-638, https://doi.org/https://doi.org/10.1130/0091-7613(1996)024<0635:PROTBO>2.3.CO;2.

Garzanti, E. 2017. The Maturity Myth In Sedimentology and Provenance AnalysiS. *Journal of Sedimentary Research*, **87**, 353-365, https://doi.org/https://doi.org/10.2110/jsr.2017.17.

Garzanti, E., Vermeesch, P., Andò, S., Lustrino, M., Padoan, M. and Vezzoli, G. 2014. Ultra-long distance littoral transport of Orange sand and provenance of the Skeleton Coast Erg (Namibia). *Marine Geology*, **357**, 25-36, https://doi.org/https://doi.org/10.1016/j.margeo.2014.07.005.

Gehrels, G., Valencia, V. and Pullen, A. 2006. Detrital zircon geochronology by laser-ablation multicollector ICPMS at the Arizona LaserChron Center. *The Paleontological Society Papers*, **12**, 67-76, https://doi.org/DOI: https://doi.org/10.1017/S1089332600001352.

Gower, C.F. 1996. The evolution of the Grenville Province in eastern Labrador, Canada. *Geological Society, London, Special Publications*, **112**, 197-218, https://doi.org/https://doi.org/10.1144/GSL.SP.1996.112.01.11.

Guerrot, C. and Peucat, J. 1990. U-Pb geochronology of the Upper Proterozoic Cadomian orogeny in the northern Armorican Massif, France. *Geological Society, London, Special Publications*, **51**, 13-26, https://doi.org/https://doi.org/10.1144/GSL.SP.1990.051.01.02.

Gutiérrez-Alonso, G., Fernández-Suárez, J., Collins, A.S., Abad, I. and Nieto, F. 2005. Amazonian Mesoproterozoic basement in the core of the Ibero-Armorican Arc: 40Ar/39Ar detrital mica ages complement the zircon's tale. *Geology*, **33**, 637-640, https://doi.org/https://doi.org/10.1130/G21485AR.1.

Hancock, J.M. 1989. Sea-level changes in the British region during the Late Cretaceous. *Proceedings of the Geologists' Association*, **100**, 565-IN561.

Haq, B.U. 2014. Cretaceous eustasy revisited. *Global and Planetary change*, **113**, 44-58, https://doi.org/https://doi.org/10.1016/j.gloplacha.2013.12.007.

Harrison, T.M., Célérier, J., Aikman, A.B., Hermann, J. and Heizler, M.T. 2009. Diffusion of 40Ar in muscovite. *Geochimica et Cosmochimica Acta*, **73**, 1039-1051, https://doi.org/https://doi.org/10.1016/j.gca.2008.09.038.

Hartley, A. 1995. Sedimentology of the Cretaceous Greensand, Quadrants 48 and 49, North Celtic Sea Basin: a progradational shoreface deposit. *Geological*

Society, London, Special Publications, **93**, 245-257, https://doi.org/https://doi.org/10.1144/GSL.SP.1995.093.01.17.

Henderson, B.J., Collins, W.J., Murphy, J.B., Gutierrez-Alonso, G. and Hand, M. 2016. Gondwanan basement terranes of the Variscan–Appalachian orogen: Baltican, Saharan and West African hafnium isotopic fingerprints in Avalonia, Iberia and the Armorican Terranes. *Tectonophysics*, **681**, 278-304, https://doi.org/https://doi.org/10.1016/j.tecto.2015.11.020.

Henrique-Pinto, R., Guilmette, C., Bilodeau, C. and McNicoll, V. 2017. Evidence for transition from a continental forearc to a collisional pro-foreland basin in the eastern Trans-Hudson Orogen: Detrital zircon provenance analysis in the Labrador Trough, Canada. *Precambrian Research*, **296**, 181-194, https://doi.org/https://doi.org/10.1016/j.precamres.2017.04.035.

Hesselbo, S.P., Ogg, J.G. & Ruhl., M. 2020. The Jurassic Period. *In*: Gradstein, F.M., Ogg, J.G., Schmitz, M.D. and Ogg, G.M. (eds) *The Geologic Time Scale 2020*. Amsterdam: Elsevier, 955 – 1021.

Hibbard, J.P., Van Staal, C.R. and Rankin, D.W. 2007. A comparative analysis of pre-Silurian crustal building blocks of the northern and the southern Appalachian orogen. *American Journal of Science*, **307**, 23-45, https://doi.org/https://doi: 10.2475/01.2007.02.

Hietpas, J., Samson, S., Moecher, D. and Chakraborty, S. 2011. Enhancing tectonic and provenance information from detrital zircon studies: assessing terrane-scale sampling and grain-scale characterization. *Journal of the Geological Society, London*, **168**, 309-318, https://doi.org/https://doi.org/10.1144/0016-76492009-163.

Higgs, K. and Beese, A. 1986. A Jurassic microflora from the Colbond Clay of Cloyne, County Cork. *Irish Journal of Earth Sciences*, 99-109.

Hoffman, P.F. 1990. Subdivision of the Churchill Province and the extent of the Trans-Hudson Orogen. *The Early Proterozoic Trans-Hudson Orogen of North America*, 15-39.

Hounslow, M. and Ruffell, A. 2006. Triassic: seasonal rivers, dusty deserts and saline lakes. *The Geology of England & Wales*. Geological Society of London., 295-325.

ISPSG, I.S.P.S.G. 2019. *The Standard Stratigraphic Nomenclature of Offshore Ireland: An Integrated Lithostratigraphic, Biostratigraphic and Sequence Stratigraphic Framework, Dublin: Irish Petroleum Infrastructure Programme (PIP).*

Jones, S.M., White, N., Clarke, B.J., Rowley, E. and Gallagher, K. 2002. Present and past influence of the Iceland Plume on sedimentation. *Geological Society, London, Special Publications*, **196**, 13-25, https://doi.org/https://doi.org/10.1144/GSL.SP.2002.196.01.02.

Keeley, M. 1995. New evidence of Permo-Triassic rifting, onshore southern Ireland, and its implications for Variscan structural inheritance. *Geological Society, London, Special Publications*, **91**, 239-253, https://doi.org/https://doi.org/10.1144/GSL.SP.1995.091.01.12.

Kessler, L. and Sachs, S.D. 1995. Depositional setting and sequence stratigraphic implications of the Upper Sinemurian (Lower Jurassic) sandstone interval, North Celtic Sea/St George's Channel Basins, offshore Ireland. *Geological Society, London, Special Publications*, **93**, 171-192, https://doi.org/https://doi.org/10.1144/GSL.SP.1995.093.01.13.

Kirstein, L., Davies, G. and Heeremans, M. 2006. The petrogenesis of Carboniferous–Permian dyke and sill intrusions across northern Europe. *Contributions to Mineralogy and Petrology*, **152**, 721-742, https://doi.org/https://doi.org/10.1007/s00410-006-0129-9.

Kuiper, K., Deino, A. and Hilgen, F. 2008. Synchronizing Rock Clocks of Earth History. *Synchronizing rock clocks of Earth history: Science*, **320**, 500-504, https://doi.org/https://doi:10.1126/science.1154339.

Lafuente, B., Downs, R., Yang, H. and Stone, N. 2015. The power of databases: the RRUFF project. *In*: Armbruster, T. and Danisi, R. (eds) *Highlights in mineralogical crystallography*. De Gruyter, Berlin, Germany 1, 30, https://doi.org/https://doi.org/10.1515/9783110417104-003.

Lee, J.-Y., Marti, K., Severinghaus, J.P., Kawamura, K., Yoo, H.-S., Lee, J.B. and Kim, J.S. 2006. A redetermination of the isotopic abundances of atmospheric Ar. *Geochimica et Cosmochimica Acta*, **70**, 4507-4512, https://doi.org/https://doi.org/10.1016/j.gca.2006.06.1563.

Long, C.B., Max, M.D. and Yardley, B.W. 1983. Compilation Caledonian metamorphic map of Ireland *Regional Trends in the Geology of the Appalachian-Caledonian-Hercynian-Mauritanide Orogen*. Springer, 221-233, https://doi.org/https://doi.org/10.1007/978-94-009-7239-1_21.

Ludwig, K. 2012. Isoplot 3.75-4.15 manual. *A Geochronological Toolkit for Microsoft Excel*, **4**, 1-70.

Mange, M.A. and Maurer, H. 1992. *Heavy minerals in colour*. Springer Science & Business Media.

Mange, M.A. and Wright, D.T. 2007. *Heavy minerals in use*. Elsevier.

Max, M., Barber, A. and Martinez, J. 1990. Terrane assemblage of the Leinster Massif, SE Ireland, during the Lower Palaeozoic. *Journal of the Geological Society, London*, **147**, 1035-1050, https://doi.org/https://doi.org/10.1144/gsjgs.147.6.1035.

McAteer, C.A., Daly, J.S., Flowerdew, M.J., Whitehouse, M.J. and Monaghan, N.M. 2014. Sedimentary provenance, age and possible correlation of the Iona Group SW Scotland. *Scottish Journal of Geology*, **50**, 143-158, https://doi.org/https://doi.org/10.1144/sjg2013-019.

McConnell, B., Rogers, R. and Crowley, Q. 2016. Sediment provenance and tectonics on the Laurentian margin: implications of detrital zircons ages from the Central Belt of the Southern Uplands–Down–Longford Terrane in Co. Monaghan, Ireland. *Scottish Journal of Geology*, **52**, 11-17, https://doi.org/https://doi.org/10.1144/sjg2015-013.

McDowell, F.W., McIntosh, W.C. and Farley, K.A. 2005. A precise 40Ar–39Ar reference age for the Durango apatite (U–Th)/He and fission-track dating standard. *Chemical Geology*, **214**, 249-263.

Meere, P.A. and Mulchrone, K.F. 2006. Timing of deformation within Old Red Sandstone lithologies from the Dingle Peninsula, SW Ireland. *Journal of the Geological Society, London*, **163**, 461-469, https://doi.org/https://doi.org/10.1144/0016-764905-099.

Miles, A.J. and Woodcock, N. 2018. A combined geochronological approach to investigating long lived granite magmatism, the Shap granite, UK. *Lithos*, **304**, 245-257, https://doi.org/https://doi.org/10.1016/j.lithos.2018.02.012.

Millson, J. 1987. The Jurassic evolution of the Celtic Sea basins. *Conference on petroleum geology of North West Europe. 3*, 599-610.

Min, K., Mundil, R., Renne, P.R. and Ludwig, K.R. 2000. A test for systematic errors in 40Ar/39Ar geochronology through comparison with U/Pb analysis of a 1.1-Ga rhyolite. *Geochimica et Cosmochimica Acta*, **64**, 73-98, https://doi.org/https://doi.org/10.1016/S0016-7037(99)00204-5.

Monaghan, A. and Pringle, M. 2004. 40Ar/39Ar geochronology of Carboniferous-Permian volcanism in the Midland Valley, Scotland. *Geological Society, London, Special Publications*, **223**, 219-241, https://doi.org/https://doi.org/10.1144/GSL.SP.2004.223.01.10.

Monster, M.W.L. 2016. *Multi-method palaeointensity data of the geomagnetic field during the past 500 kyrs from European volcanoes.* UU Dept. of Earth Sciences.

Morton, A. 1984. Stability of detrital heavy minerals in Tertiary sandstones from the North Sea Basin. *Clay minerals*, **19**, 287-308.

Morton, A., Knox, R. and Frei, D. 2016. Heavy mineral and zircon age constraints on provenance of the Sherwood Sandstone Group (Triassic) in the eastern Wessex Basin, UK. *Proceedings of the Geologists' Association*, **127**, 514-526, https://doi.org/https://doi.org/10.1016/j.pgeola.2016.06.001.

Morton, A.C. 1982. The provenance and diagenesis of Palaeogene sandstones of southeast England as indicated by heavy mineral analysis. *Proceedings of the Geologists' Association*, **93**, 263-274.

Morton, A.C. and Hallsworth, C. 1994. Identifying provenance-specific features of detrital heavy mineral assemblages in sandstones. *Sedimentary Geology*, **90**, 241-256, https://doi.org/https://doi.org/10.1016/0037-0738(94)90041-8.

Murphy, J.B., Nance, R.D., Gabler, L.B., Martell, A. and Archibald, D.A. 2019. Age, geochemistry and origin of the Ardara appinite plutons, northwest Donegal, Ireland. *Geoscience Canada: Journal of the Geological Association of*

Canada/Geoscience Canada: journal de l'Association Géologique du Canada, **46**, 31-48, https://doi.org/https://doi.org/10.12789/geocanj.2019.46.144.

Murphy, N.J. and Ainsworth, N.R. 1991. Stratigraphy of the Triassic, Lower Jurassic and Middle Jurassic (Aalenian) from the Fastnet Basin, offshore south-west Ireland. *Marine and Petroleum Geology*, **8**, 417-429, https://doi.org/https://doi.org/10.1016/0264-8172(91)90064-8.

Nance, R.D., Neace, E.R., Braid, J.A., Murphy, J.B., Dupuis, N. and Shail, R.K. 2015. Does the Meguma terrane extend into SW England? *Geoscience Canada*, 61-76, https://doi.org/https://doi.org/10.12789/geocanj.2014.41.056.

Nance, R.D., Murphy, J.B., Strachan, R.A., Keppie, J.D., Gutiérrez-Alonso, G., Fernández-Suárez, J., Quesada, C., Linnemann, U., D'lemos, R. and Pisarevsky, S.A. 2008. Neoproterozoic-early Palaeozoic tectonostratigraphy and palaeogeography of the peri-Gondwanan terranes: Amazonian v. West African connections. *Geological Society, London, Special Publications*, **297**, 345-383, https://doi.org/https://doi.org/10.1144/SP297.17.

Nasdala, L., Corfu, F., Schoene, B., Tapster, S.R., Wall, C.J., Schmitz, M.D., Ovtcharova, M., Schaltegger, U., Kennedy, A.K. and Kronz, A. 2018. GZ 7 and GZ 8–Two Zircon Reference Materials for SIMS U-Pb Geochronology. *Geostandards and Geoanalytical Research*, **42**, 431-457, https://doi.org/ https://doi.org/10.1111/ggr.12239.

Nauton-Fourteu, M., Tyrrell, S., Morton, A., Mark, C., O'Sullivan, G.J. and Chew, D.M. 2020. Constraining recycled detritus in quartz-rich sandstones: insights from a multi-proxy provenance study of the Mid-Carboniferous, Clare Basin, western Ireland. *Basin Research*, https://doi.org/https://doi.org/10.1111/bre.12469.

Naylor, D. and Shannon, P. 1982. *Geology of offshore Ireland and west Britain*, United Kingdom.

Naylor, D. and Shannon, P. 2011. *Petroleum geology of Ireland*. Dunedin Academic Press Limited.

O'Connor, P. and Brück, P. 1978. Age and origin of the Leinster Granite. *Journal of Earth Sciences*, 105-113.

O'Reilly, B.M., Shannon, P.M. and Vogt, U. 1991. Seismic studies in the North Celtic Sea Basin: implications for basin development. *Journal of the Geological Society, London*, **148**, 191-195, https://doi.org/https://10.1144/gsjgs.148.1.0191.

O'Sullivan, G., Chew, D., Kenny, G., Henrichs, I. and Mulligan, D. 2020. The trace element composition of apatite and its application to detrital provenance studies. *Earth-Science Reviews*, **201**, 103044, https://doi.org/https://doi.org/10.1016/j.earscirev.2019.103044.

Pascoe, R., Power, M. and Simpson, B. 2007. QEMSCAN analysis as a tool for improved understanding of gravity separator performance. *Minerals engineering*, **20**, 487-495, https://doi.org/https://doi.org/10.1016/j.mineng.2006.12.012.

Paton, C., Hellstrom, J., Paul, B., Woodhead, J. and Hergt, J. 2011. Iolite: Freeware for the visualisation and processing of mass spectrometric data. *Journal of Analytical Atomic Spectrometry*, **26**, 2508-2518, https://doi.org/https://10.1039/C1JA10172B.

Payton, C.E. 1977. *Seismic stratigraphy: applications to hydrocarbon exploration*. American Association of Petroleum Geologists Tulsa, OK.

Petrie, S., Brown, J., Granger, P. and Lovell, J. 1989. Mesozoic history of the Celtic Sea basins. *Extensional Tectonics and Stratigraphy of the North Atlantic Margins American Association of Petroleum Geologists Memoirs*, **46**, 433-445.

Petrus, J.A. and Kamber, B.S. 2012. VizualAge: A Novel Approach to Laser Ablation ICP-MS U-Pb Geochronology Data Reduction. *Geostandards and Geoanalytical Research*, **36**, 247-270, https://doi.org/https://10.1111/j.1751-908X.2012.00158.x.

Pointon, M.A., Cliff, R.A. and Chew, D.M. 2012. The provenance of Western Irish Namurian Basin sedimentary strata inferred using detrital zircon U–Pb LA-ICP-MS geochronology. *Geological Journal*, **47**, 77-98.

Pollock, J.C., Hibbard, J.P. and van Staal, C.R. 2012. A paleogeographical review of the peri-Gondwanan realm of the Appalachian orogen. *Canadian Journal of Earth Sciences*, **49**, 259-288, https://doi.org/https://doi.org/10.1139/e11-049.

Pothier, H.D., Waldron, J.W., Schofield, D.I. and DuFrane, S.A. 2015. Peri-Gondwanan terrane interactions recorded in the Cambrian–Ordovician detrital zircon geochronology of North Wales. *Gondwana Research*, **28**, 987-1001, https://doi.org/https://doi.org/10.1016/j.gr.2014.08.009.

Rainbird, R.H., Hamilton, M.A. and Young, G.M. 2001. Detrital zircon geochronology and provenance of the Torridonian, NW Scotland. *Journal of the Geological Society, London*, **158**, 15-27, https://doi.org/https://doi.org/10.1144/jgs.158.1.15.

Rawson, P. and Riley, L. 1982. Latest Jurassic-Early Cretaceous events and the "late Cimmerian unconformity" in North Sea area. *AAPG Bulletin*, **66**, 2628-2648, https://doi.org/https://doi.org/10.1306/03B5AC87-16D1-11D7-8645000102C1865D.

Robinson, K., Shannon, P. and Young, G.M. 1981. The Fastnet Basin: An integrated analysis. *In*: Illing, L.G. and Hobson, G.D. (eds) *Petroleum Geology of the Continental Shelf of North-West Europe*. Heyden and Son Ltd, London, 444–454.

Rodriguez-Salgado, P. 2019. *Structural and Kinematic Analysis of the Celtic Sea Basins.* PhD, University College Dublin.

Rodríguez-Salgado, P., Childs, C., Shannon, P.M. and Walsh, J.J. 2019. Structural evolution and the partitioning of deformation during basin growth and inversion: A case study from the Mizen Basin Celtic Sea, offshore Ireland. *Basin Research*, https://doi.org/https://doi.org/10.1111/bre.12402.

Rowell, P. 1995. Tectono-stratigraphy of the North Celtic Sea Basin. *Geological Society, London, Special Publications*, **93**, 101-137, https://doi.org/10.1144/gsl.sp.1995.093.01.11.

Ruffell, A. and Shelton, R. 1999. The control of sedimentary facies by climate during phases of crustal extension: examples from the Triassic of onshore and offshore England and Northern Ireland. *Journal of the Geological Society, London*, **156**, 779-789, https://doi.org/https://doi.org/10.1144/gsjgs.156.4.0779.

Ruffell, A.H. and Rawson, P.F. 1994. Palaeoclimate control on sequence stratigraphic patterns in the late Jurassic to mid-Cretaceous, with a case study

from Eastern England. *Palaeogeography, Palaeoclimatology, Palaeoecology*, **110**, 43-54, https://doi.org/https://doi.org/10.1016/0031-0182(94)90109-0.

Schoene, B. and Bowring, S.A. 2006. U–Pb systematics of the McClure Mountain syenite: thermochronological constraints on the age of the 40 Ar/39 Ar standard MMhb. *Contributions to Mineralogy and Petrology*, **151**, 615.

Shannon, P. 1991. The development of Irish offshore sedimentary basins. *Journal of the Geological Society, London*, **148**, 181-189, https://doi.org/https://doi.org/10.1144/gsjgs.148.1.0181.

Shannon, P. 1996. Current and future potential of oil and gas exploration in Ireland. *In*: Glennie, K. and Hurst, A. (eds) *AD1995-NW Europe's Hydrocarbon Industry. Geol. Soc, London*. Journal of the Geological Society, London, 51-62.

Shannon, P. and Naylor, D. 1998. An assessment of Irish offshore basins and petroleum plays. *Journal of Petroleum Geology*, **21**, 125-152, https://doi.org/https://doi.org/10.1111/j.1747-5457.1998.tb00651.x.

Shannon, P.M. 1995. Permo-Triassic development of the Celtic Sea region, offshore Ireland. *Geological Society London Special Publication*, **91**, 215-237, https://doi.org/https://doi.org/10.1144/GSL.SP.1995.091.01.11.

Shannon, P.M., Corcoran, D.V. and Haughton, P.D.W. 2001. The petroleum exploration of Ireland's offshore basins: introduction. *Geological Society, London, Special Publications*, **188**, 1-8, https://doi.org/https://10.1144/gsl.sp.2001.188.01.01.

Sibuet, J.C., Dyment, J., Bois, C., Pinet, B. and Ondreas, H. 1990. Crustal structure of the Celtic Sea and Western Approaches from gravity data and deep seismic profiles: constraints on the formation of continental basins. *Journal of Geophysical Research: Solid Earth*, **95**, 10999-11020, https://doi.org/https://doi.org/10.1029/JB095iB07p10999.

Sláma, J., Košler, J., Condon, D.J., Crowley, J.L., Gerdes, A., Hanchar, J.M., Horstwood, M.S., Morris, G.A., Nasdala, L. and Norberg, N. 2008. Plešovice zircon—a new natural reference material for U–Pb and Hf isotopic microanalysis. *Chemical Geology*, **249**, 1-35, https://doi.org/https://doi.org/10.1016/j.chemgeo.2007.11.005.

Smith, W.D., Darling, J., Bullen, D., Lasalle, S., Pereira, I., Moreira, H., Allen, C.J. and Tapster, S. 2019. Zircon perspectives on the age and origin of evolved S-type granites from the Cornubian Batholith, Southwest England. *Lithos*, **336**, 14-26, https://doi.org/https://doi.org/10.1016/j.lithos.2019.03.025.

Somerville, I.D., Strogen, P. and Jones, G.L. 1992. Biostratigraphy of Dinantian limestones and associated volcanic rocks in the Limerick Syncline, Ireland. *Geological Journal*, **27**, 201-220, https://doi.org/https://doi.org/10.1002/gj.3350270302.

Soper, N. and Hutton, D. 1984. Late Caledonian sinistral displacements in Britain: implications for a three-plate collision model. *Tectonics*, **3**, 781-794, https://doi.org/https://10.1029/TC003i007p00781.

Stampfli, G.M. and Kozur, H.W. 2006. Europe from the Variscan to the Alpine cycles. *Journal of the Geological Society, London*, **32**, 57-82, https://doi.org/https://doi.org/10.1144/GSL.MEM.2006.032.01.04.

Strachan, R., Collins, A., Buchan, C., Nance, R., Murphy, J. and D'Lemos, R. 2007. Terrane analysis along a Neoproterozoic active margin of Gondwana: insights from U–Pb zircon geochronology. *Journal of the Geological Society, London*, **164**, 57-60, https://doi.org/https://doi.org/10.1144/0016-76492006-014.

Taber, D., Vickers, M. and Winn, R. 1995. The definition of the Albian 'A'Sand reservoir fairway and aspects of associated gas accumulations in the North Celtic Sea Basin. *Geological Society, London, Special Publications*, **93**, 227-244, https://doi.org/https://doi.org/10.1144/GSL.SP.1995.093.01.16.

Tate, M. and Dobson, M. 1988. Syn-and post-rift igneous activity in the Porcupine Seabight Basin and adjacent continental margin W of Ireland. *Geological Society, London, Special Publications*, **39**, 309-334, https://doi.org/https://doi.org/10.1144/GSL.SP.1988.039.01.28.

Thomson, S.N., Gehrels, G.E., Ruiz, J. and Buchwaldt, R. 2012. Routine low-damage apatite U-Pb dating using laser ablation–multicollector–ICPMS. *Geochemistry, Geophysics, Geosystems*, **13**, https://doi.org/https://10.1029/2011GC003928.

Todd, S. 2015. Structure of the Dingle Peninsula, SW Ireland: evidence for the nature and timing of Caledonian, Acadian and Variscan tectonics. *Geological Magazine*, **152**, 242-268, https://doi.org/https://doi.org/10.1017/S0016756814000260.

Tyrrell, S. 2005. *Investigations of Sandstone Provenance.* PhD University College Dublin.

Tyrrell, S., Haughton, P.D. and Daly, J.S. 2007. Drainage reorganization during breakup of Pangea revealed by in-situ Pb isotopic analysis of detrital K-feldspar. *Geology*, **35**, 971-974, https://doi.org/https://doi.org/10.1130/G4123A.1.

Van der Voo, R. 1988. Paleozoic paleogeography of North America, Gondwana and intervening. displaced terranes: Comparisons of palaeomagnetism with paleoclimatology and biogeographical patterns. *Geological Society of America Bulletin*, **100**, 411-423, https://doi.org/https://doi.org/10.1130/0016-7606(1988)100<0311:PPONAG>2.3.CO;2.

van Staal, C.R., Sullivan, R.W. and Whalen, J.B. 1996. Provenance of tectonic history of the Gander Zone in the Caledonian/Appalachian Orogen: Implications for the origin and assembly of Avalon. *In*: Damian Nance, M.D.T. (ed.) *Avalonian and Related Peri-Gondwanan Terranes of the Circum-North Atlantic*. Geological Society of America, 347-367.

Vermeesch, P. 2018. IsoplotR: A free and open toolbox for geochronology. *Geoscience Frontiers*, **9**, 1479-1493, https://doi.org/https://doi.org/10.1016/j.gsf.2018.04.001.

Vermeesch, P., Resentini, A. and Garzanti, E. 2016. An R package for statistical provenance analysis. *Sedimentary Geology*, **336**, 14-25, https://doi.org/https://doi.org/10.1016/j.sedgeo.2016.01.009.

Vermeesch, P., Rittner, M., Petrou, E., Omma, J., Mattinson, C. and Garzanti, E. 2017. High throughput petrochronology and sedimentary provenance analysis by automated phase mapping and LAICPMS. *Geochemistry, Geophysics, Geosystems*, **18**, 4096-4109, https://doi.org/https://doi.org/10.1002/2017GC007109.

Waldron, J.W., Schofield, D.I. and Murphy, J.B. 2019a. Diachronous Paleozoic accretion of peri-Gondwanan terranes at the Laurentian margin. *Geological Society, London, Special Publications*, **470**, 289-310, https://doi.org/https://doi.org/10.1144/SP470.11.

Waldron, J.W., Floyd, J.D., Simonetti, A. and Heaman, L.M. 2008. Ancient Laurentian detrital zircon in the closing Iapetus ocean, Southern Uplands terrane, Scotland. *Geology*, **36**, 527-530, https://doi.org/https://doi.org/10.1130/G24763A.1.

Waldron, J.W., Schofield, D.I., White, C.E. and Barr, S.M. 2011. Cambrian successions of the Meguma Terrane, Nova Scotia, and Harlech Dome, North Wales: dispersed fragments of a peri-Gondwanan basin? *Journal of the Geological Society, London*, **168**, 83-98, https://doi.org/https://doi.org/10.1144/0016-76492010-068.

Waldron, J.W., Schofield, D.I., Pearson, G., Sarkar, C., Luo, Y. and Dokken, R. 2019b. Detrital zircon characterization of early Cambrian sandstones from East Avalonia and SE Ireland: implications for terrane affinities in the peri-Gondwanan Caledonides. *Geological Magazine*, **156**, 1217-1232, https://doi.org/https://doi.org/10.1017/S0016756818000407.

Waldron, J.W., Schofield, D.I., Dufrane, S.A., Floyd, J.D., Crowley, Q.G., Simonetti, A., Dokken, R.J. and Pothier, H.D. 2014. Ganderia–Laurentia collision in the Caledonides of Great Britain and Ireland. *Journal of the Geological Society, London*, **171**, 555-569, https://doi.org/https://doi.org/10.1144/jgs2013-131.

Warrington, G. and Ivimey-Cook, H. 1992. Triassic. *In*: Cope, J., Ingham, J. and Rawson, P. (eds) *Atlas of palaeogeography and lithofacies.* Geological Society of London Memoir, 97-106.

Welch, M.J. and Turner, J.P. 2000. Triassic–Jurassic development of the St. George's Channel basin, offshore Wales, UK. *Marine and Petroleum Geology*, **17**, 723-750, https://doi.org/https://doi.org/10.1016/S0264-8172(00)00017-9.

White, C., Palacios, T., Jensen, S. and Barr, S. 2012. Cambrian–Ordovician acritarchs in the Meguma terrane, Nova Scotia, Canada: Resolution of early Paleozoic stratigraphy and implications for paleogeography. *GSA Bulletin*, **124**, 1773-1792, https://doi.org/https://doi.org/10.1130/B30638.1.

Wiedenbeck, M., Alle, P., Corfu, F., Griffin, W., Meier, M., Oberli, F.v., Quadt, A.v., Roddick, J. and Spiegel, W. 1995. Three natural zircon standards for U-Th-Pb, Lu-Hf, trace element and REE analyses. *Geostandards newsletter*, **19**, 1-23, https://doi.org/https://doi.org/10.1111/j.1751-908X.1995.tb00147.x.

Winn Jr, R.D. 1994. Shelf sheet-sand reservoir of the Lower Cretaceous Greensand, North Celtic Sea Basin, offshore Ireland. *AAPG Bulletin*, **78**, 1775-1789, https://doi.org/https://doi.org/10.1306/A25FF28D-171B-11D7-8645000102C1865D.

Yang, P., Welford, J.K., Peace, A.L. and Hobbs, R. 2020. Investigating the Goban Spur rifted continental margin, offshore Ireland, through integration of new seismic reflection and potential field data. *Tectonophysics*, **777**, 228364, https://doi.org/https://doi.org/10.1016/j.tecto.2020.228364.

Zhang, X., Pease, V., Omma, J. and Benedictus, A. 2015. Provenance of Late Carboniferous to Jurassic sandstones for southern Taimyr, Arctic Russia: a comparison of heavy mineral analysis by optical and QEMSCAN methods. *Sedimentary Geology*, **329**, 166-176, https://doi.org/https://doi.org/10.1016/j.sedgeo.2015.09.008.

Ziegler, P.A. 1990. *Geological Atlas of Western and Central Europe*. 2 ed. Shell Internationale Petroleum Maatschappij B.V. 239pp.

Ziegler, P.A., Cloetingh, S. and van Wees, J.-D. 1995. Dynamics of intra-plate compressional deformation: the Alpine foreland and other examples. *Tectonophysics*, **252**, 7-59.

Zimmermann, S., Mark, C., Chew, D. and Voice, P.J. 2018. Maximising data and precision from detrital zircon U-Pb analysis by LA-ICPMS: The use of core-rim ages and the single-analysis concordia age. *Sedimentary Geology*, **375**, 5-13, https://doi.org/https://doi.org/10.1016/j.sedgeo.2017.12.020.

Fig. 1 Map of the present-day study area with onshore and offshore bathymetry (EMODnet 2018). Stars are coloured by basin and mark sampled well locations. CBB; Cardigan Bay Basin, DG; Dalradian Supergroup, LM; Leinster Massif, MB; Munster Basin, WM; Welsh Massif, CM; Cornubia Massif, SM; Scottish Massif, PB; Porcupine Basin, SB; Slyne Basin, NCSB; North Celtic Sea Basin, SCSB; South Celtic Sea Basin, SGCB; Saint George's Channel Basin, FB; Fastnet Basin, GS; Goban Spur Basin, MCT; Monian Composite Terrane (Nance *et al.* 2015; Waldron *et al.* 2019b).

Fig. 2 Summary of the Mesozoic lithostratigraphy of the Fastnet Basin, NCSB and SGCB. Lithostratigraphy adapted from Tyrrell (2005) and interpretations from well logs. Red circles indicate sample locations. New group nomenclature is taken from a new standard lithostratigraphic framework for offshore Ireland (ISPSG 2019). Old group nomenclature and sea level data are taken from Murphy and Ainsworth (1991); Ewins and Shannon (1995); Shannon (1995); Welch and Turner (2000); Hounslow and Ruffell (2006).

Fig. 3 Total heavy mineral abundance of samples from the Middle Jurassic to Upper Cretaceous sequences of the NCSB and SGCB. Note that three samples contained 130 – 200 HM grains and should be interpreted with caution (See Table 2). Samples without an asterisk are drill cuttings samples.

Fig. 4 PCA biplot of HMA results from Middle Jurassic to Upper Cretaceous samples. (B) Biplot of GZi *vs* MZi ratios. Symbols used in both figures represent the same samples. NC-UJ; NCSB Upper Jurassic, SG-UJ; SGCB Upper Jurassic, SG-MJ; SGCB Middle Jurassic samples, NC-LC; NCSB Lower Cretaceous, SG-UC; SGCB Upper Cretaceous, NC-UC; NCSB Upper Cretaceous.

Table 1. *Single grain age groups based on significant orogenic events where P = Population. Groupings are defined as discussed in Potential Sediment Sources section.*

Fig. 5 (A) KDE diagrams of detrital zircon from the Middle to Upper Jurassic. (B) Sample locations. For further details see Table 3 supplementary information. (C) Representative source samples from Waldron *et al.* (2008), Chew *et al.* (2010), Waldron *et al.* (2014) and (Pothier *et al.* 2015).

Fig. 6 (A) Lower and Upper Cretaceous detrital zircon results summarised in KDE diagrams from the NCSB and SGCB. For classification of the population groupings, see Table 1. (B) Well locations for sampling. For further details see Table 3 supplementary information.

Fig. 7 Apatite trace element SVM biplots with corresponding KDE U-Pb apatite diagrams from Jurassic and Cretaceous samples. (A) SG16 from the Upper Cretaceous. (B) NC22 from the Upper Cretaceous (C) SG5 core sample from the Middle Jurassic. ALK = alkali-rich igneous rocks; IM = mafic I-type granitoids and mafic igneous rocks; LM=low-medium grade metamorphic and metasomatic; HM=partial-melts/leucosomes/high-grade metamorphic; S=S-type granitoids and high aluminium saturation index (ASI) 'felsic' I-types; UM = ultramafic rocks including carbonatites, lherzolites and pyroxenites (O'Sullivan et al. 2020). For further details see Table 4 for U-Pb and Table 5 for trace element information.

Fig. 8 ^{40}Ar-^{39}Ar dating of detrital white mica samples from Jurassic and Cretaceous sediments of the NCSB. For further details see Table 6 supplementary information.

Fig. 9 Bajocian palaeoenvironmental reconstruction after Shannon and Naylor (1998) , Naylor and Shannon (2011), Keeley (1995). Dark brown – topographical highs, light brown – topographical lows, light blue – shallow marine environments, navy – deeper marine, red – igneous centre. Cross-hatch polygons mark basin boundaries and red arrows indicate sediment transport direction. MB; Munster Basin, LM; Leinster Massif, CM; Cornubian Massif, LBH; London Brabant High, WM; Welsh Massif, MCT; Monian Composite Terrane, PH; Porcupine High.

Fig. 10 Palaeoenvironmental model during the Kimmeridgian and Oxfordian after Shannon and Naylor (1998), Naylor and Shannon (2011), Keeley (1995). Dark brown – topographical highs, light brown – topographical lows, light blue – shallow marine environments, navy – deeper marine, red – igneous centre. Crosshatch polygons mark basin boundaries and red arrows indicate sediment transport direction. MB; Munster Basin, LM; Leinster Massif, CM; Cornubian Massif, LBH; London Brabant High, WM; Welsh Massif, MCT; Monian Composite Terrane, PH; Porcupine High.

Fig. 11 Palaeoenvironmental reconstruction during the Early Cretaceous (Hauterivian) after Rodríguez-Salgado *et al.* (2019), (Naylor and Shannon 2011), Ewins and Shannon (1995), Ainsworth *et al.* (1985). Dark brown – topographical highs, light brown – topographical lows, light blue – shallow marine environments, navy - deeper marine, red – igneous centre. Cross hatch polygons mark basin boundaries and red arrows indicate sediment transport direction. MB; Munster Basin, LM; Leinster Massif, CM; Cornubian Massif, LBH; London Brabant High, WM; Welsh Massif, MCT; Monian Composite Terrane, PH; Porcupine High.

Fig. 12 Palaeoenvironmental reconstruction during the Late Cretaceous (Campanian) after Naylor and Shannon (2011), (Shannon 1991) and Hancock (1989). Sediment routing is indicated by red arrows. Dark brown – topographical highs, light brown – topographical lows, light blue – shallow marine environments, navy – deeper marine, red – igneous centre. Cross hatch polygons mark basin boundaries and red arrows indicate sediment transport direction. MB; Munster Basin, LM; Leinster Massif, CM; Cornubian Massif, LBH; London Brabant High, WM; Welsh Massif, MCT; Monian Composite Terrane, PH; Porcupine High.

Figure 1

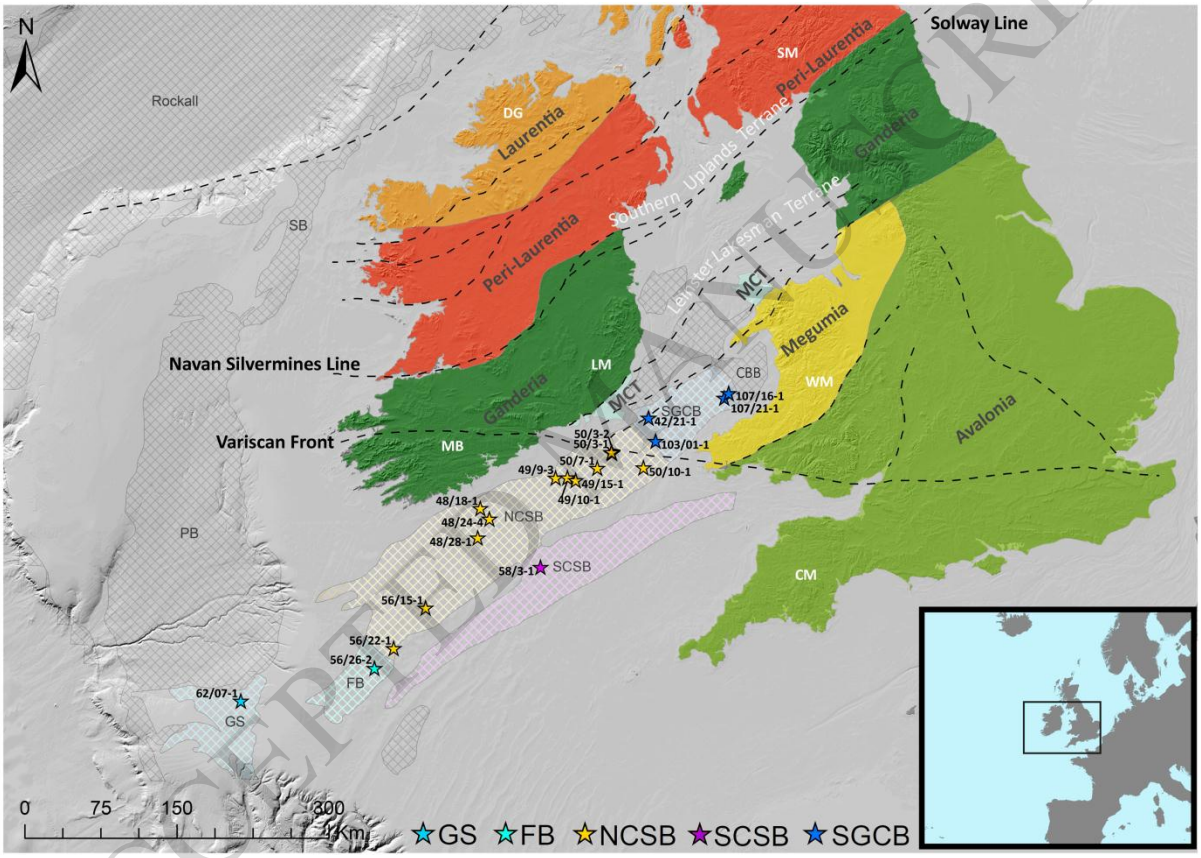

Figure 2

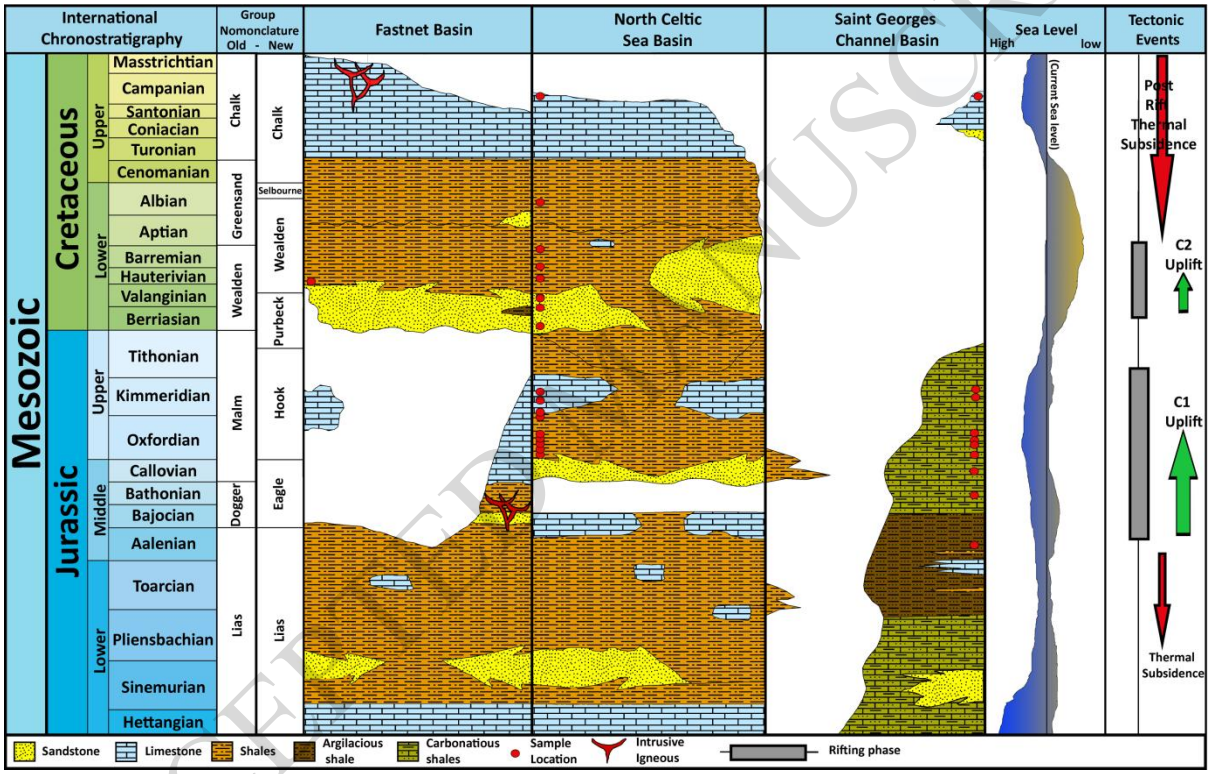

Figure 3

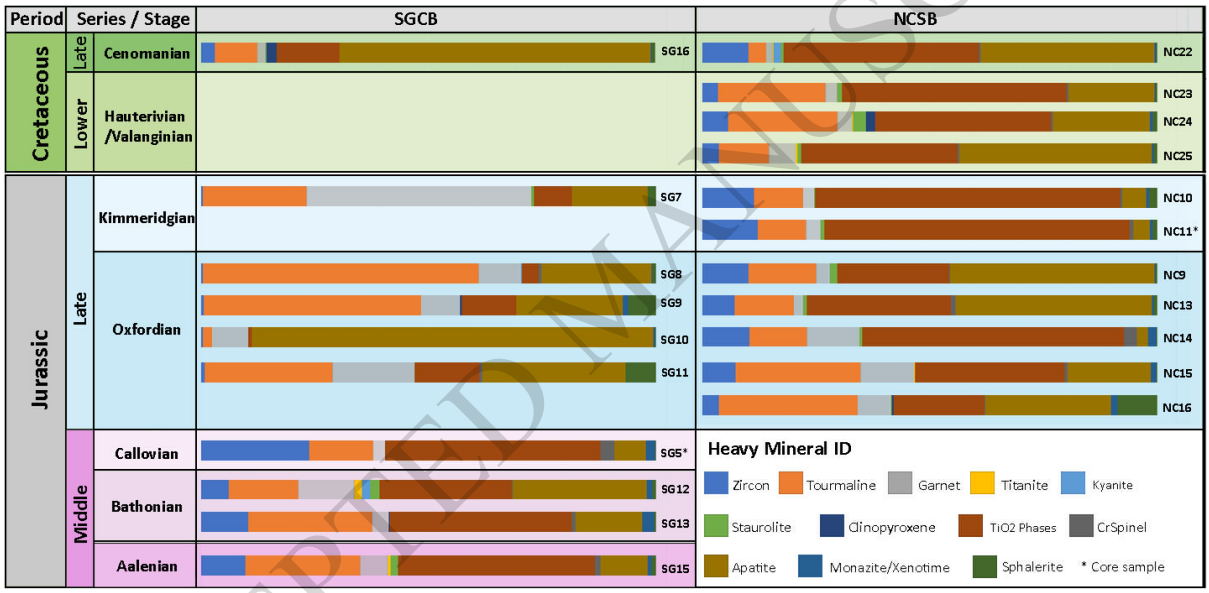

Figure 4

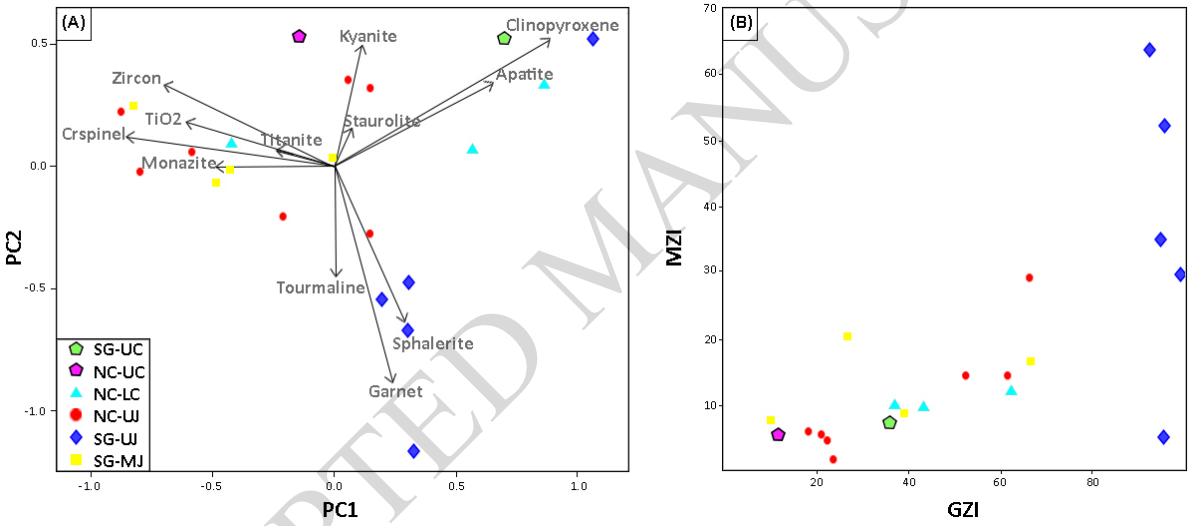

Figure 5

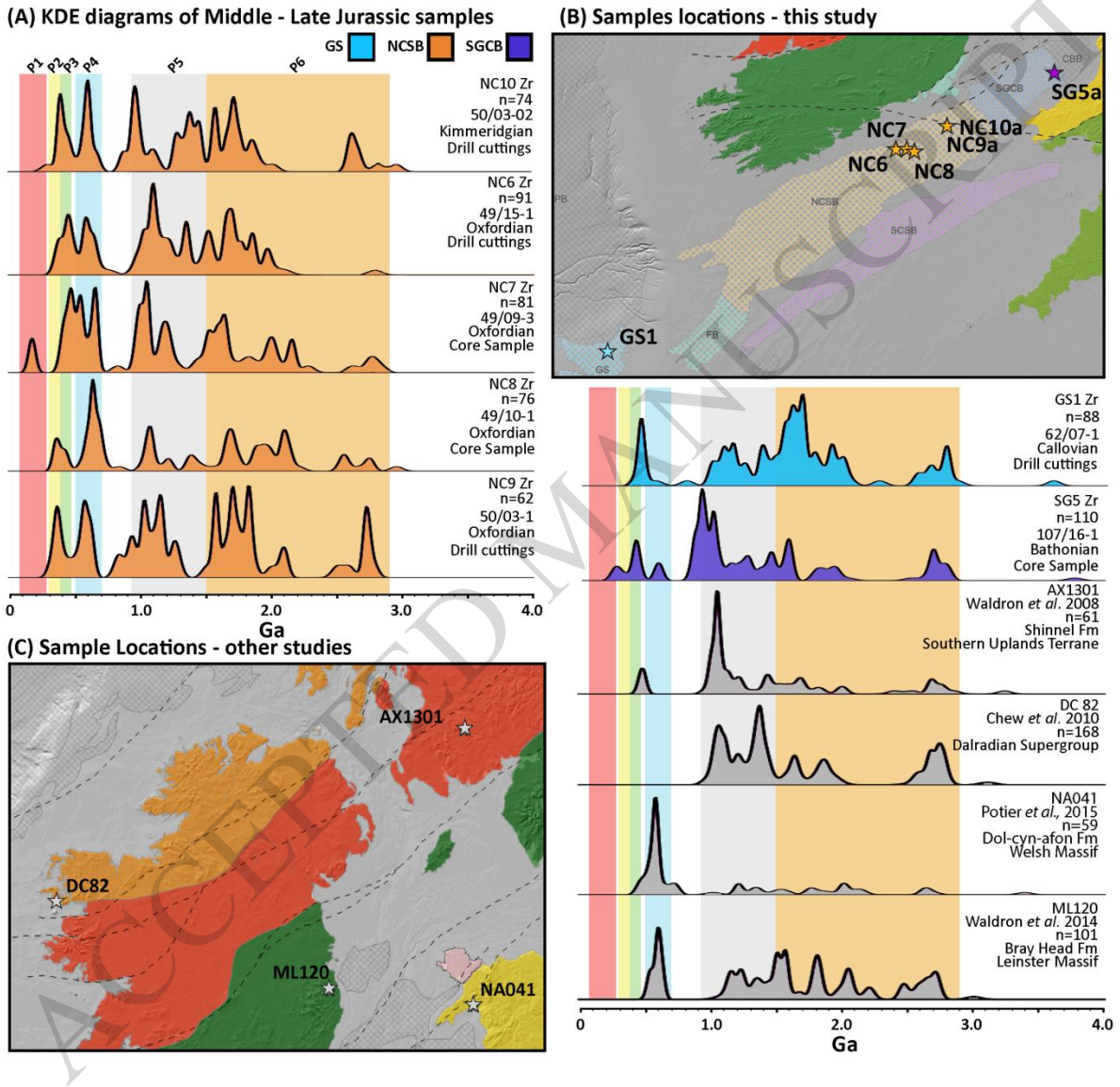

Figure 6

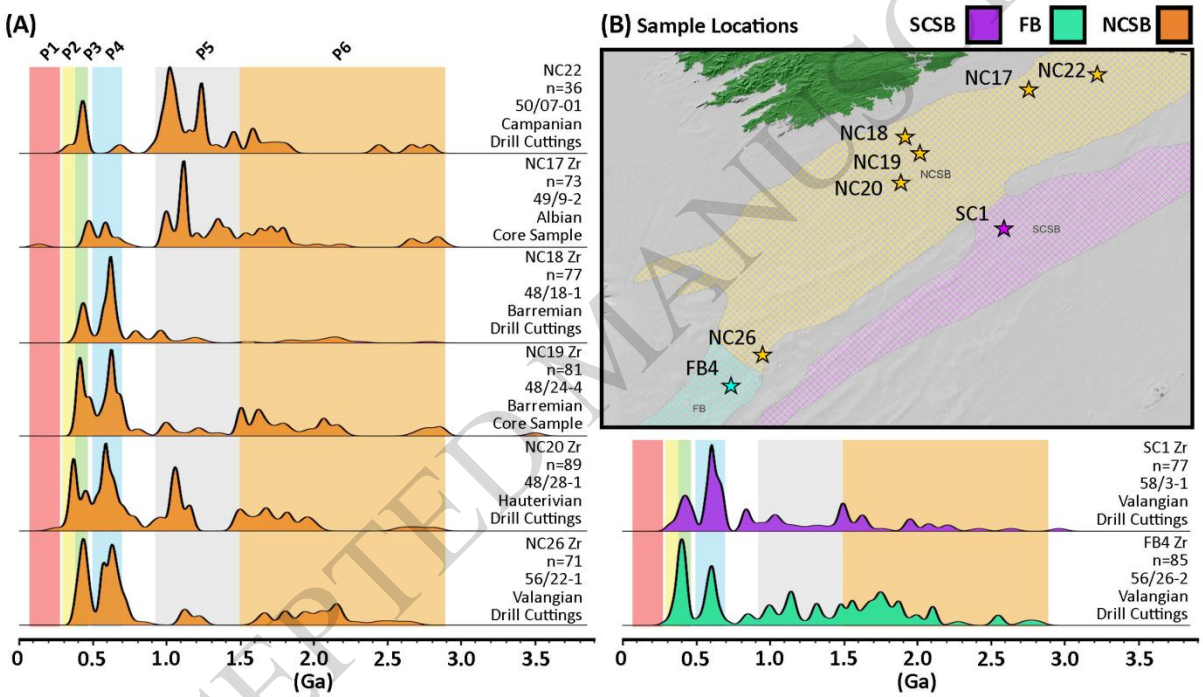

Figure 7

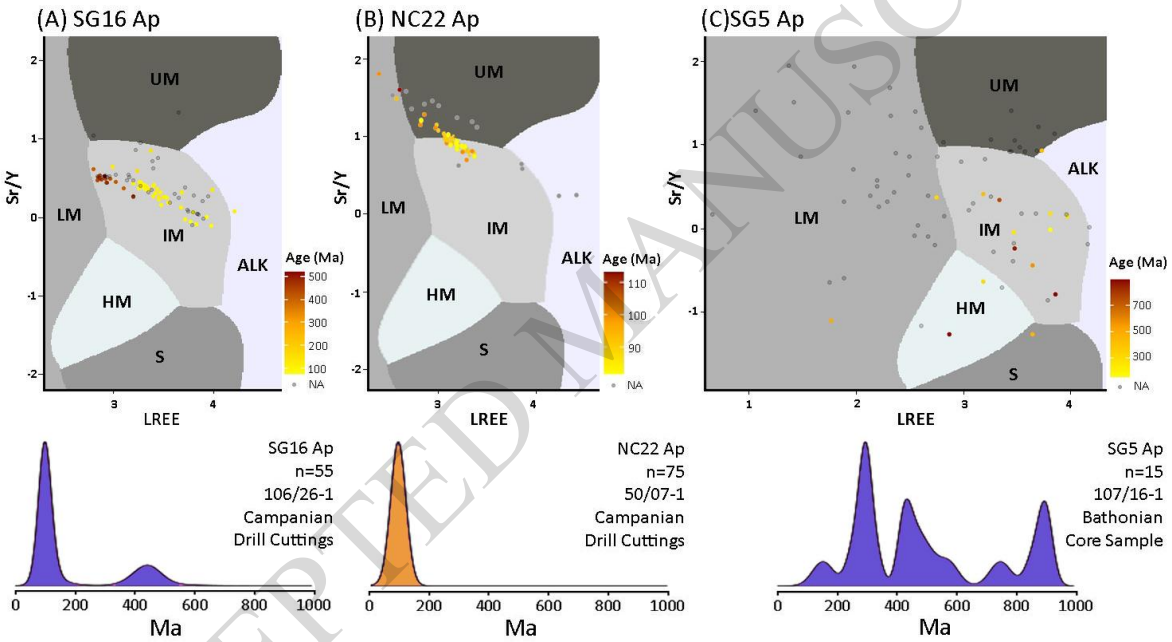

Figure 8

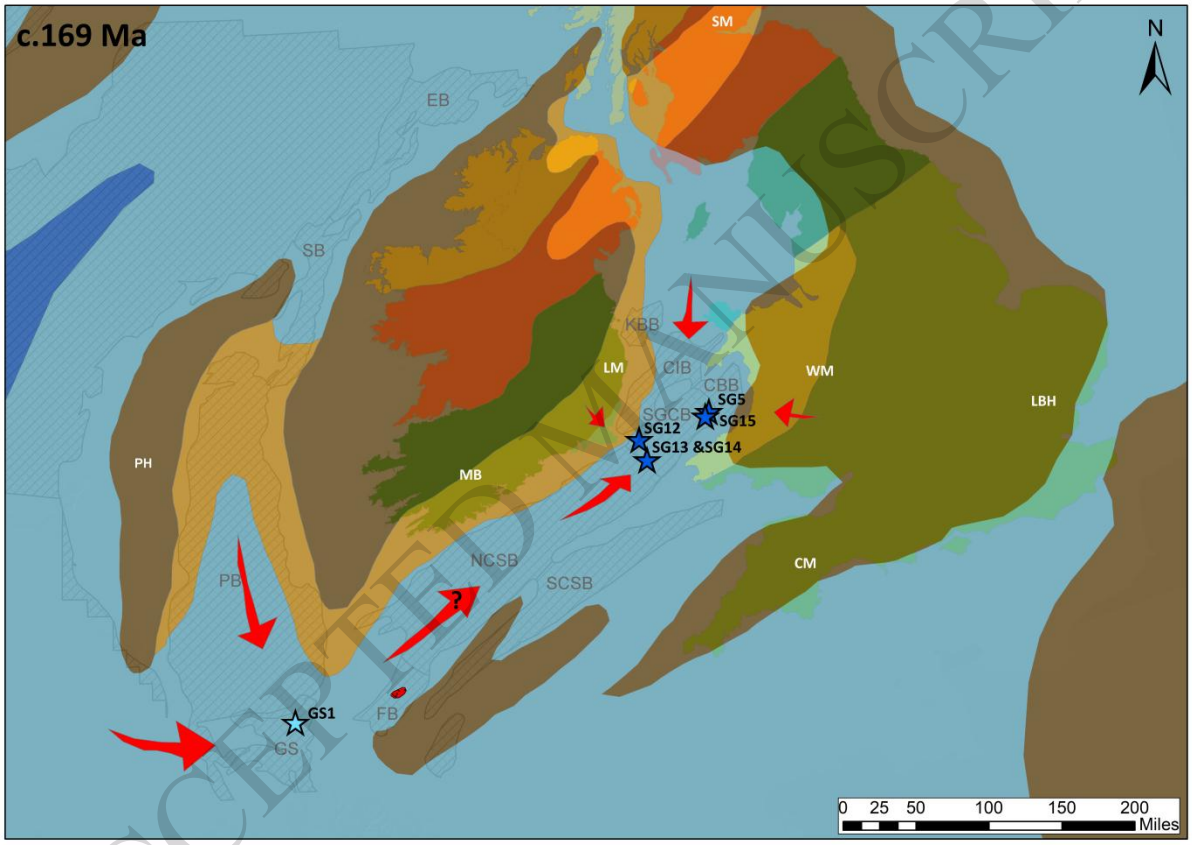

Figure 9

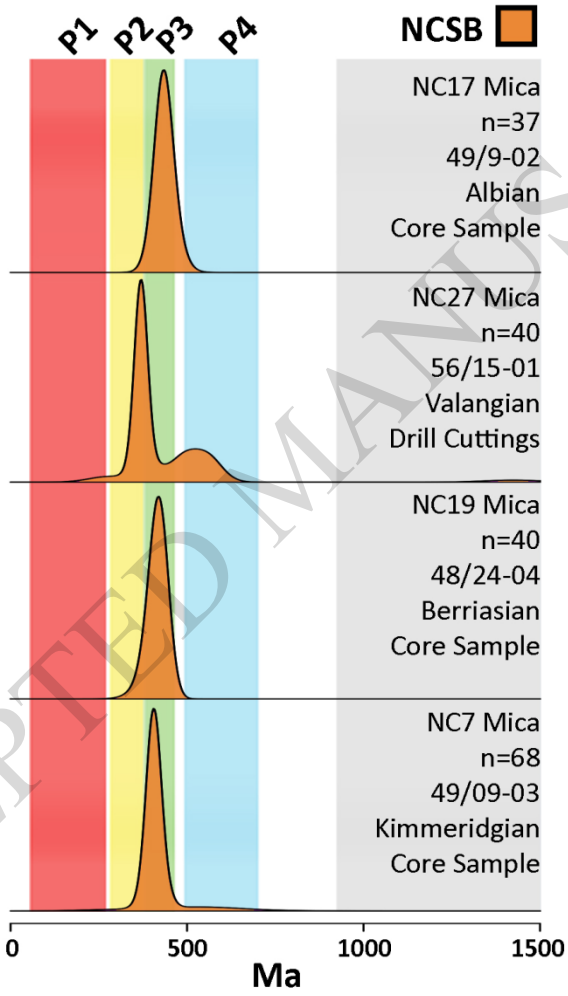

Figure 10

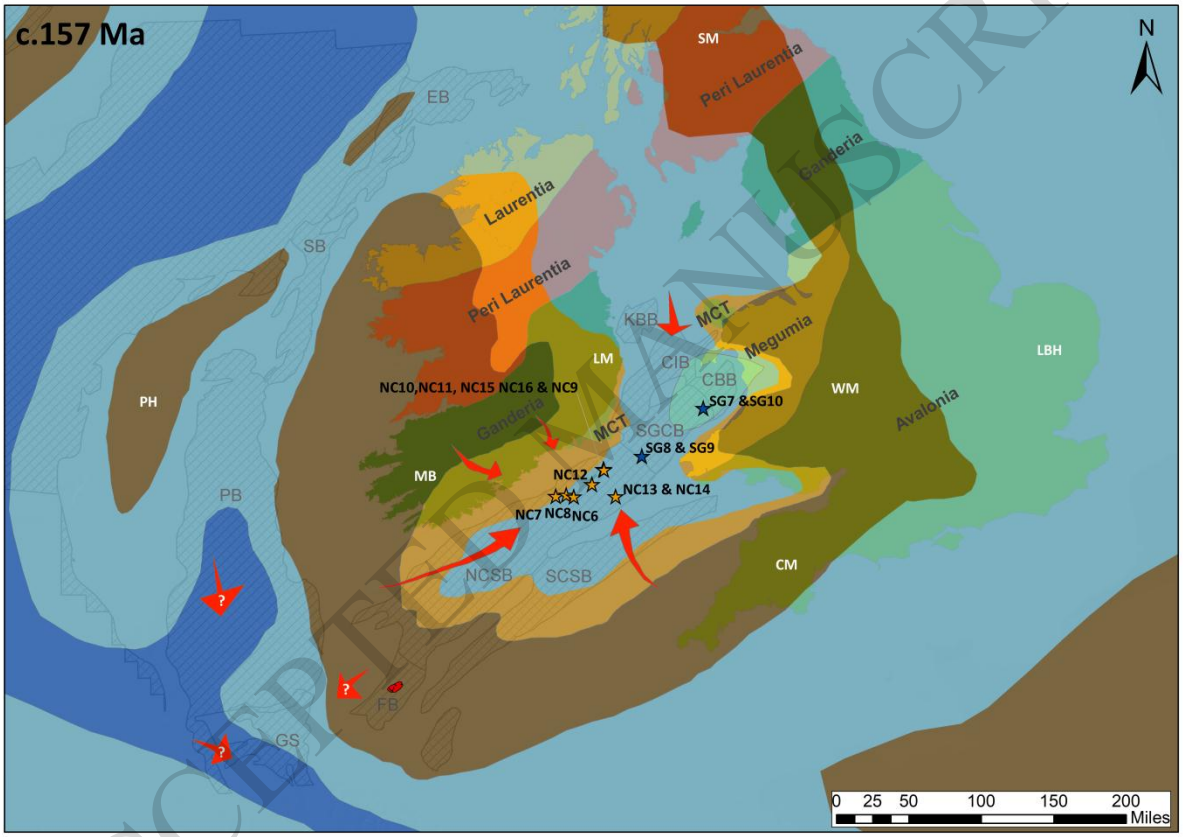

Figure 11

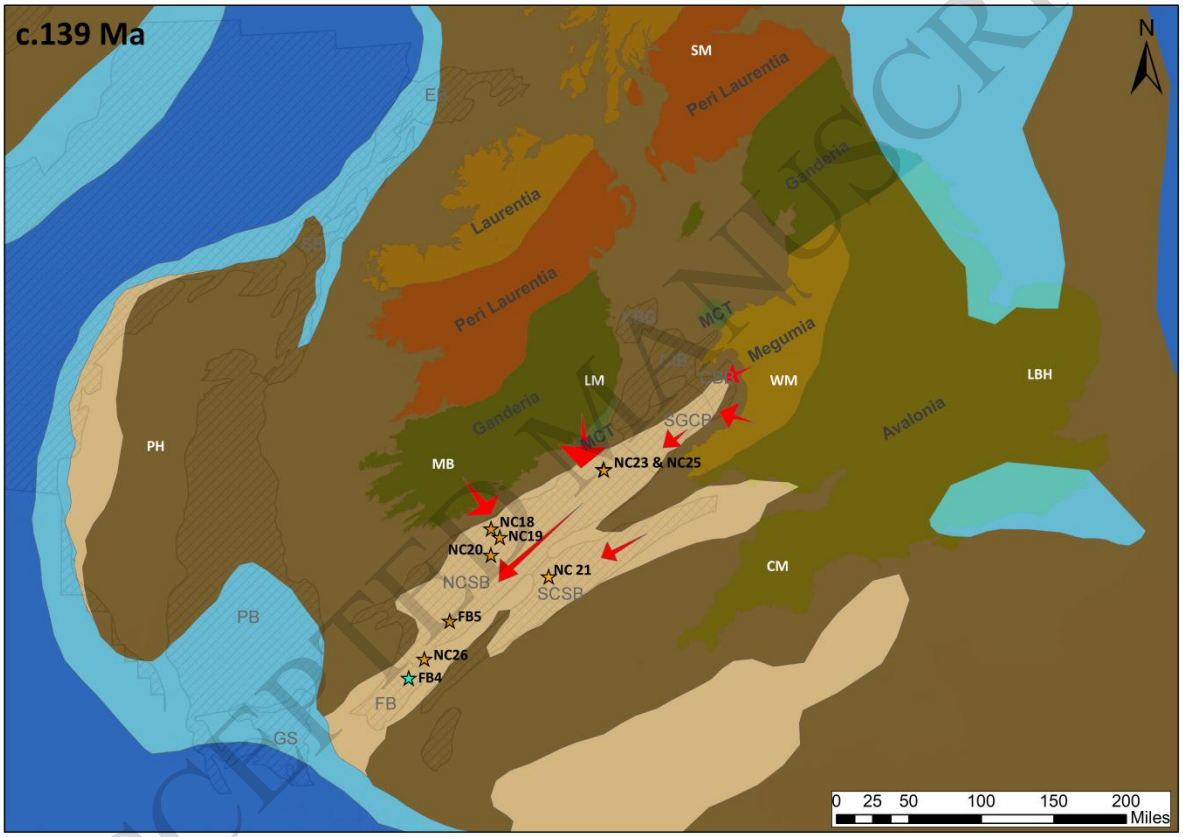

Figure 12